CHEMISTRY & SUSTAINABILITY
CHEMSUSCHEM
ENERGY & MATERIALS

Accepted Article

Title: Iridium-based Catalysts for Electrocatalytic Water Splitting

Authors: chao wang, feifei lan, zhenfeng he, xiaofeng xie, yuhong zhao, hua hou, Li Guo, murugadoss vignesh, Qian Shao, Hu Liu, Qiang Gao, Tao Ding, and Zhanhu Guo

To be cited as: *ChemSusChem* 10.1002/cssc.201802873

Link to VoR: http://dx.doi.org/10.1002/cssc.201802873

A Journal of ChemPubSoc Europe

WILEY-VCH www.chemsuschem.org

10.1002/cssc.201802873

REVIEW

Iridium-based Catalysts for Solid Polymer Electrolyte Electrocatalytic Water Splitting

Chao Wang,* [a] Feifei Lan,[a] Zhenfeng He, [b] Xiaofeng Xie, [c] Yuhong Zhao,[a] Hua Hou,[a] Li Guo,[a] Vignesh Murugadoss,[d] Hu Liu,[d], [e] Qian Shao,[f] Qiang Gao,* [g] Tao Ding,* [h] Renbo Wei,*[i] Zhanhu Guo* [d]

Prof. C. Wang, F. Lan, Prof. Y. Zhao, Prof. H. Hou, Prof. L. Guo
[a]Advanced Energy Materials and Systems Institute,
College of Materials Science and Engineering,
North University of China, Taiyuan, 030051 China
E-mail: wangchao_nuc@126.com (C. W)
Prof. Z. He
[b]National Demonstration Center for Experimental Chemical Engineering Comprehensive Education,
School of Chemical Engineering and Technology,
North University of China, Taiyuan 030051, China
Prof. X. Xie
[c] INET, Tsinghua University, Beijing, 100084, China
E-mail: xiexf@tsinghua.edu.cn (X. Xie)
v. Murugadoss, Dr. H. Liu, Prof. Dr. Z. Guo
[d]Integrated Composites Laboratory (ICL),
Department of Chemical & Biomolecular Engineering,
University of Tennessee, Knoxville, TN 37996 USA
E-mail: zguo10@utk.edu (Z. Guo)
H. Liu
[e]Key Laboratory of Materials Processing and Mold (Zhengzhou University),
Ministry of Education; National Engineering Research Center for
Advanced Polymer Processing Technology,
Zhengzhou University, Zhengzhou, 450002, China
Prof. Q. Shao
[f]College of Chemical and Environmental Engineering,
Shandong University of Science and Technology,
Qingdao, Shandong, 266590, China
Dr. Q. Gao
[g]Center for Nanophase Materials Sciences,
Oak Ridge National Laboratory, P.O. Box 2008, Oak Ridge, TN 37831, USA
E-mail: gaoq@ornl.gov (Q.G)
Prof. T. Ding
[h]College of Chemistry and Chemical Engineering,
Henan University, Kaifeng 475004, China
E-mail: dingtao@henu.edu.cn (T.D.)
Prof. R. Wei
Research Branch of Advanced Functional Materials, School of Materials and Energy,
University of Electronic Science and Technology of China, Chengdu, 611731, China
E-mail: weirb10@uestc.edu.cn
NOTE: Chao Wang and Feifei Lan contributed equally to this work

10.1002/cssc.201802873

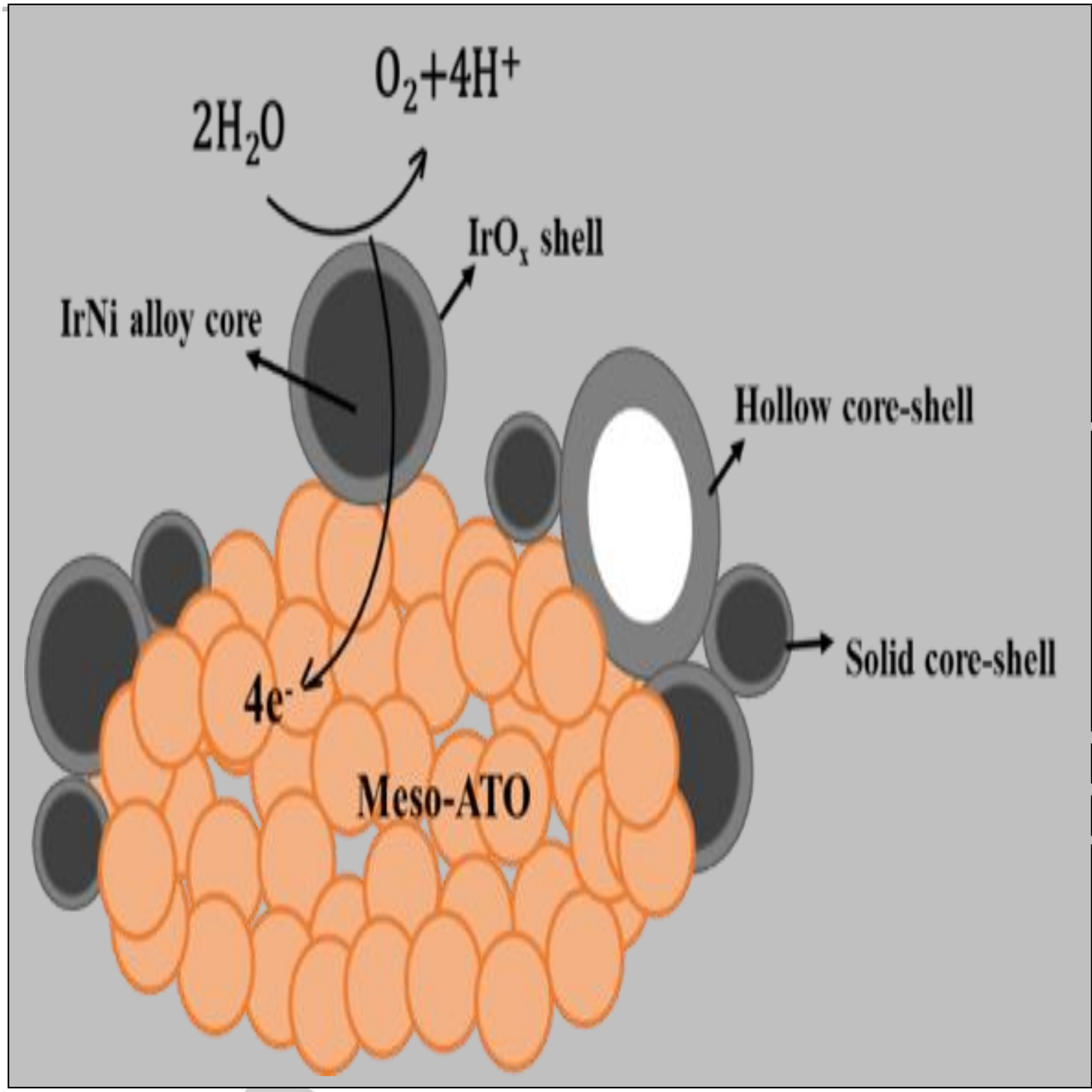

 10.1002/cssc.201802873

WILEY-VCH

REVIEW

Abstract: Chemical energy conversion/storage through water splitting for hydrogen production has been recognized as the ideal solution to the transient nature of renewable energy sources. Solid polymer electrolyte (SPE) water electrolysis is one of the most practical ways to produce pure H_2. Electrocatalysts are key materials in the SPE water electrolysis. At anode side, electrode materials catalyzing the oxygen evolution reaction (OER) require properties. Among the reported materials, only iridium presents high activity and is more stable. In this article, an application overview of single iridium metal and its oxide catalysts; binary, ternary and multi-component catalysts of iridium oxides; and supported composite catalysts for the OER in SPE water electrolysis is presented. Two main strategies to improve the activity of an electrocatalyst system, *i.e.,* increasing the number of active sites and the intrinsic activity of each active site were reviewed with detailed examples. The challenges and perspectives in this field are also discussed.

1. Introduction

Climate change, pollution and the scarcity of fossil fuels require our society to pursue clean and renewable energy sources. Hydrogen has been considered as the most abundant and promising energy carrier because of its high efficiency and no environmental pollution, etc. Nowadays water electrolysis is the most attractive renewable resource for hydrogen production. Electricity can be derived from solar energy, wind energy, water conservancy, tidal energy, and geothermal energy, etc [1-5].
Regarding water electrolysis, solid polymer electrolyte (SPE) water electrolysis have been extensively investigated [5-8]. The main advantages of SPE water electrolysis are fast kinetics of the cathode hydrogen evolution reaction (HER) and high-voltage efficiencies at high current densities. The main challenge arising from high energy consumption limits its large-scale industrial applications, mainly owing to the higher over-potential of the sluggish oxygen evolution reaction (OER). Moreover, the lack of stable electrocatalysts remains challenging. Under operation conditions, few electrocatalysts can present adequate stability. Noble IrO_2 has excellent corrosion resistance and high catalytic activity for OER [8], whereas high price of IrO_2 has limited their applications. In the appropriate synthesis protocol, selecting right material to dope or support the catalyst can effectively reduce the amount of anode metals, and meanwhile can improve the corrosion resistance of the electrode.
The main feature of SPE water electrolysis technology lies in replacing the traditional caustic solution electrolytes with SPE. Solid polymer is perfluorosulfonic acid proton exchange membrane (commonly Nafion). Sulfonic acid groups can deliver hydronium ions and become a good conductor after flooding, meanwhile hydrogen ions have a good conduction. Proton exchange membrane (PEM) satisfies numerous physical criteria, including 1) good ionic conductivity and thermal conductivity; 2) poor electronic conductivity; 3) good chemical and mechanical stability; 4) good thermal stability; 5) ease of manufacture and production in the form of large surface membranes of homogeneous thickness; and 6) low gas solubility [9]. PEM serves as both electrolyte and separator. The SPE water electrolysis principle diagram of the structure has been shown in Figure 1.

The cathode and anode reactions occurring at the SPE water electrolysis electrodes can be described by Equations (1) and (2):

$$4e^-+4H^+\rightarrow 2H_2\uparrow \quad \text{cathode} \quad (1)$$

$$2H_2O\rightarrow 4H^++4e^-+O_2\uparrow \quad \text{anode} \quad (2)$$

Water electrolysis at anode produces O_2 and four protons near the electrode surface for each oxygen molecule. Hydrogen ions through the PEM generate H_2 gas near the cathode. The electrocatalysts are directly attached to the membrane to form the SPE composite membrane electrode. The selective separation of the proton membrane enables the integrated structure to reduce the voltage drop of the electrolyte, and thus has high energy efficiency and improves the current efficiency. The only liquid used in the electrolyzer is deionized water, which will reduce the corrosion of equipment and extend the service life. Nevertheless, the higher production cost limits its large-scale applications.

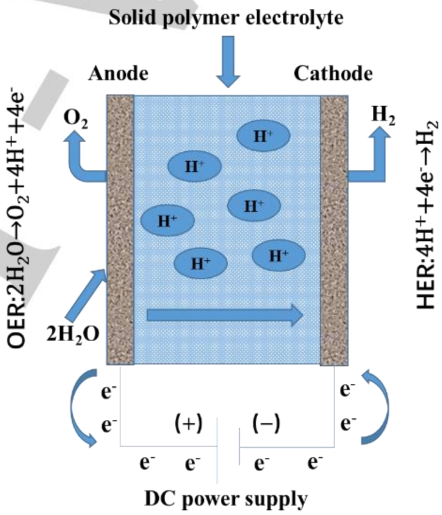

Figure 1. Cross-section diagram of a SPE water electrolysis cell.

Chao Wang, born in 1987 in Beijing, engages mainly in polymer flame retardant materials, fuel cells and ion-exchange membrane research, hosts one National Science Foundation for Young Scientists of China and participated in the Key International S&T Cooperation Projects of the Ministry of Science and Technology.

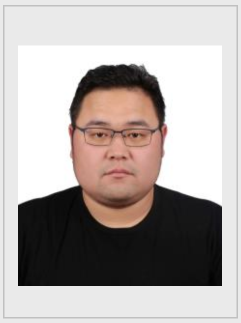

To evaluate the performance of the catalysts, the most important parameters are their activity and stability. The key factors restricting the commercialization of H_2 production are the cost and performance of the catalysts. Thus, the research and application of catalysts are directly related to the commercial prospect of electrolyzing hydrogen from solid polymer electrolytes.

In the SPE water electrolysis cell, the Pt metal catalyst with acid stability and hydrogen evolution catalytic activity is the most suitable cathode electrocatalyst because of the strong acid nature (equivalent to 10% H_2SO_4) after the PEM absorbs water. The cathode HER in SPE water electrolysis has a small over-potential. The widely used cathodes to date are noble metal Pt catalysts, including Pt/C[10-13], PtNPs/CNFs (Pt nanoparticles/carbon nanofibers),[14], Pt/GNF (Platinum supported by graphitic nano-fibers) [15] Pt-Fe, or Pt-C[16], because Pt element has an incompletely filled d-orbital, the outermost electron structure $5_{d9}6_{s1}$ and a suitable atomic radius of 177 pm favor the adsorption of H atoms and the desorption of H_2, *i.e.,* the faster the kinetics of electron reduction to H_2, the lower the activation energy is, and the lower the hydrogen evolution potential becomes. To reduce the amount of Pt and increase its electrochemical specific surface area, it has been usually prepared as Pt particles and supported on a porous carbon substrate *e.g.,* platinum-on-carbon (Pt/C) catalyst particles.

In this minireview, we summarized (in Table 1) and discussed the current issues and recent developments of IrO_2-based catalysts for the OER in SPE water electrolysis to extract a guideline for developing electrocatalysts with high activity, low cost and high stability.

2. Progress in Catalysts of Oxygen Evolution Reaction（OER）

2.1. Catalyst of Oxygen Evolution Reaction（OER）

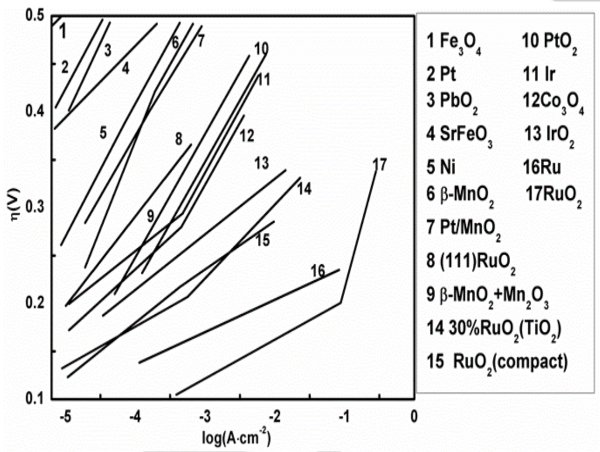

Figure 2. Schematic over-potential vs log i curves for oxygen evolution on various metals and (or) oxides from acid solutions. Modified from ref[19].

The over-potential of OER is much higher than that of the HER [17, 18]. Accordingly, the OER has been intensively studied to elucidate the reaction mechanism, stability issues and to reduce the over-potential of the OER electrode during water electrolysis. The standard electrode potential for OER is 1.23 V vs. RHE but most metal electrodes dissolve before reaching this potential, only few metals and their oxides present adequate stability. Figure 2 shows the oxygen evolution polarization curves of different metals and their oxides in acidic solution.[19] It can be seen from the figure 2 that the oxygen evolution current values of different material surfaces can differ by several orders of magnitude at a certain overpotential. Ru and RuO_2 electrodes are the best electrocatalyst for oxygen generation in acidic solution. Figure 3 shows the relationship between the metal oxide over-potential and the enthalpy of oxidation of different valence oxides at a current density of 1 m A cm^{-2}.[19-21] Obviously, RuO_2 and IrO_2 are promising oxygen anode catalysts which are at the top of the curve. Both have the most suitable metal-oxygen bond strength and are the most conducive to the OER with the smallest over-potential.[22-25]

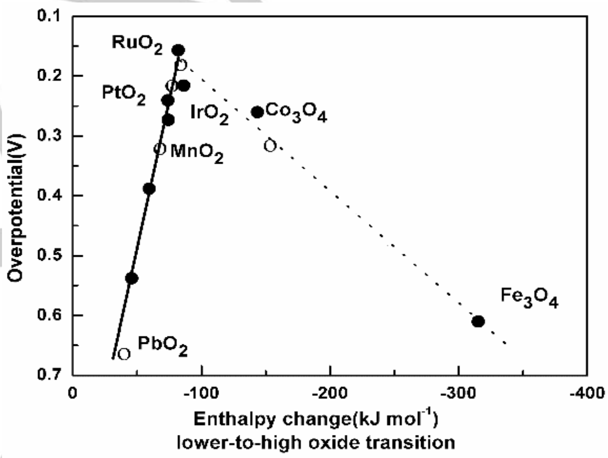

Figure 3. Relationship between metal oxide overpotential and enthalpy of conversion of different valence oxides at 1 mA · cm $^{-2}$. Modified from ref.[19]

Dimensionally stable anodes (DSAs) pure RuO_2 catalysts for OER have been reported with a very short lifetime due to the easy conversion of RuO_2 into RuO_4 at high potentials. For example, Hodnik *et al.* [26] used highly sensitive *in situ* measurements of concentration by ICP-MS to study the dissolution behaviors of Ru and its oxides at nano size scale in acidic media, for the first time, severe dissolution took place due to the OER. Moreover, OER activity was in an inverse relationship with the measured dissolution. Cherevko *et al.* [27] have demonstrated the increase of dissolution in the order of $IrO_2 \leqq RuO_2$, and hence the SPE electrolytic cell anode catalyst usually uses Ir or IrO_2 as the main active component. Previous studies [28-30] have shown that under the acidic conditions, the OER activity of IrO_2 is only slightly lower than that of RuO_2, while IrO_2 holds a service life of 20 times longer than that of RuO_2. Unfortunately, the low reserves of Ir and its high cost are the major obstacles in large scale application of SPE water electrolysis [31]. Consequently, selecting appropriate materials to dope or load the catalyst will effectively reduce the amount of anode metals, improve the corrosion resistance of the electrode, and cut its high cost.

10.1002/cssc.201802873

2.1.1. Single iridium metal and its oxide catalysts

IrO_x is the most widely used anode catalysts for OER because of its higher stability and corrosion resistance, although its electrochemical activity is slightly lower than that of RuO_2 [32-39]. Fine powders of IrO_2 can be synthesized in a variety of approaches including the Adams fusion method [40-45], colloid protocol[42,46,47] and sulfite complex route films,[48] magnetron sputtering[49-51], reduction[52], electrode deposition, and thermal decomposition[50, 53, 54]. For instance, in case of the Adams method, Wang *et al.*[44] have investigated the effect of precursor calcination temperature on the catalytic activity of the catalysts. The calcination temperature affected the catalytically active area and the electrocatalytic activity by affecting the size of the catalyst and the valence of the iridium. With the increase of temperatures, the crystallite size and crystallinity increased, the crystal specific surface area and the electrocatalytic activity decreased. The conductivity increased as the temperature increased. An increase in both crystallinity and particle size was observed with increasing the treatment time, which was known to contribute to the decrease in active surface area of the electrocatalysts. For example, Song *et al.* [42] have compared the Adams and the colloid synthesis to obtain IrO_2. Consequently, the colloid method has a better performance than Adams. The result may be due to a better dispersion of electrocatalyst in the polymer electrolyte and higher crystallinity with a higher conductivity of electrocatalysts. The more clearly discernible diffraction peaks for IrO_2 (Colloid) samples than for IrO_2 (Adams) indicated that the former possessed a slightly higher crystallinity. The average size of individual crystallites of both IrO_2 (Adams) and IrO_2 (Colloid) was about 5.5 nm, as calculated from the Scherrer equation. IrO_2 (Colloid) (1 A cm^{-2} @1.63 V) exhibited a much higher specific surface area than IrO_2 (Adams) (1 A cm^{-2} @1.66 V), indicating a better IrO_2 dispersion.

The performance for OER depends strongly on catalysts structural and morphologies [55-61]. A significant way to improve the efficiency of IrO_2 is to possess nanostructures with high specific surface area. To increase the specific surface area, a porous structure (mesoporous or macro-porous) has attached important attention. To better control the pore size and cross-linking degree, hard template or soft template with a narrow particle size distribution has been frequently employed as the structure directing agent, such as polymer microspheres (for macro-porous materials) and amphiphilic block copolymers (for mesoporous materials), *etc*. For example, Li *et al.* [55] reported a nano-porous IrO_2 catalyst with a specific surface area of 363.3 m^2 g^{-1} prepared by a facile ammonia-induced pore-forming protocol with a uniform particle size and pore size distribution. Micro/mesoporous IrO_2 prepared with NH_3 exhibited an outstanding performance (10 mA cm^{-2} @1.512 V vs.RHE) than other IrO_2 prepared without NH_3 (10 mA cm^{-2} @1.542 V vs.RHE) and commercial IrO_2 (10 mA cm^{-2} @1.551 V vs.RHE) catalyst (0.5 M H_2SO_4 , 25 ^oC, *iR* correction). The mechanism for forming nano-porous IrO_2 catalyst by an ammonia induced pore-forming method is proposed and illustrated in Fig. 4 and 5. Ortel *et al.* [56] synthesized a mesoporous iridium oxide via soft templating and evaporation-induced self-assembly, employing an amphiphilic triblock-copolymer PEO-PB-PEO. The cyclic voltammogram (CV) indicated that the templated IrO_2 film exhibits significantly larger geometric current densities than the untemplated IrO_2 film, which can be attributed to differences in the electrochemically active surface area caused by differences in the coating surface morphology induced by the pore template. The overpotential for the templated mesoporous film (1.58 V vs.RHE @100 mA cm^{-2}) is substantially lower than that for the untemplated film (1.62 V vs.RHE @100 mA cm^{-2}) for all current densities in the OER potential region(0.1 M $HClO_4$, 25 ^oC, without *iR* correction). Li *et al.*[57] utilized SBA-15 as hard template to prepare mesoporous IrO_2. The cell voltage of IrO_2 (SBA-15) anode was 1.629 V at 1 A cm^{-2}, which was about 50 mV lower than that of IrO_2 obtained with Adams protocol. In both cases, the higher activity than non-templated IrO_2 has been attributed to the more uniform dispersion, larger specific surface area and pore volume.

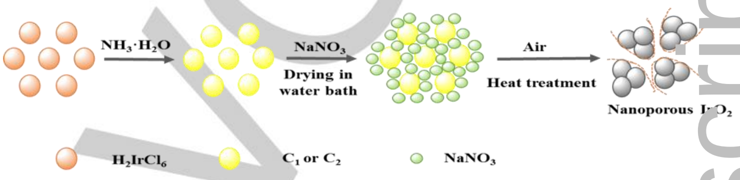

Figure 4. Schematic of the mechanism for the formation of nanoporous IrO_2 catalysts. Modified from ref.[55]

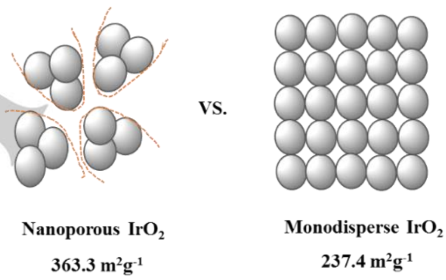

Figure 5. Specific surface area of IrO_2 (1: 100)-450 ^oC and monodispersed IrO_2. Modified from ref.[55]

Iridium nano-dendrites (Ir-ND) were synthesized by reducing H_2IrCl_6 with $NaBH_4$ in the presence of tetradecyltrimethyl ammonium bromide (TTAB) as an organic capping agent [58]. The highly branched structure of the Ir dendrites with a particle size of ~10 nm showed an enhanced OER activity. The Ir-ND have demonstrated the characteristics required for highly efficient catalysts including a large specific surface area, small particle size, combined with a high electrochemical porosity (34.2%) when compared with commercial Ir blacks [59]. The rich edges and corner atoms resulting from a dendritic structure are of great importance for high catalytic activity. Yong-Tae Kim *et al.*[62] reported the highly conductive, nanoporous architectures of an Ir oxide shell on a metallic Ir core, formed through the fast dealloying of Os from an $Ir_{25}Os_{75}$ alloy, possessed an ideal balance between activity and stability. It has been proposed that the activity-stability factor (ASF), expressed as the ratio between activity for OER and stability of the oxides, became a new key “metric” for determining the technological relevance of oxide-based anodic water electrolyzer catalysts. The nanoporous Ir/IrO_2 morphology of dealloyed $Ir_{25}Os_{75}$ shows a factor of ~30 improvement in the ASF relative to conventional Ir-based oxides, as a consequence of its nanoporous Ir-oxide/Ir-metal morphology rather than by Os-induced electronic effects on Ir surface atoms. The balance between activity and stability can be addressed through the manipulation of the material morphology. ECSA itself may not be the only factor affecting the measured OER performance, and conductivity also plays a critical role in OER performance.

2.1.2. Binary, ternary and multi-component catalysts of iridium oxides

To reduce the amount of IrO_2 loading, one common approach is to dope inexpensive metals, which can change the electronic and structural properties and improve the activity and stability [63]. The resulting electrocatalyst becomes a binary or ternary composite of iridium oxide with other metal oxides in the form of $Ir_xM_yN_zO_a$, M and N being the inexpensive metals.

Since both RuO_2 and IrO_2 are non-stoichiometric, RuO_2 is an anoxic structure (RuO_{2-x}), IrO_2 is a peroxy structure (IrO_{2+x}). The mixture of these two has a common effect of mutual matching. Therefore, the oxygen-evolving activity and stability of Ir and Ru binary oxides are much higher than that of single Ir or Ru. Extensive researches have been carried out on the Ir-Ru alloys and their oxides [64-85]. Mixed oxides formed by RuO_2 and IrO_2 retain the helpful properties of both components (high activity of RuO_2 and high stability of IrO_2). In Ir-rich mixed oxides, the presence of Ru increases the activity of Ir; or in Ru-rich mixed oxides, the presence of Ir increases the stability of Ru. Methods to form mixed Ru-Ir oxides fall into two categories: a direct and dry film formation approach (*i.e.* reactive spray deposition technology [64, 65]) or wet powder synthesis followed by an electrode formation step (*i.e.* thermal decomposition [66, 67, 76], hydrolysis method [68], Adam' s fusion [42, 43, 69-72] or sol-gel method [75, 80, 81]. The mixed oxides may be composed of homogeneous solid solutions of Ru and Ir [64-66, 70, 71] or present as IrO_2 and RuO_2 separate phases [67, 68].

Along with increasing the Ru content in $Ir_xRu_{1-x}O_2$, the average particle size and the crystallinity of catalysts increased. Generally, the $Ir_xRu_{1-x}O_2$ compounds are observed to be more active than IrO_2 and more stable than RuO_2 [64-72]. The synthesis routes have a great influence on the atomic mixing, surface segregation, and particle size. XRD and ICP-AES measurements by Mayousse *et al.* have highlighted that the quantity of Ru inserted into the oxide lattice, via the Adams fusion method, can be finely controlled without any phase separation [43]. Siracusano *et al.* applied a pre-leaching procedure to achieve high degree of surface purity and promote an enrichment of Ir on the outer surface [72]. The Ir content in the Ru-based catalyst composition contributes to its stability against dissolution without increasing the over-potential at its surface. Cheng *et al.* [70] observed that RuO_2 as an anodic electrocatalyst is unstable, with the potential rising to 8 V_{SCE} at about 20000 s. $Ir_{0.2}Ru_{0.8}O_2$ shows a higher stability than RuO_2, and the potential is lower than 2 V_{SCE} even the time approaches 40000 s. An increase of the performance has been well documented upon Ru insertion [67]. Felix *et al.* [71] further proved that the addition of RuO_2 to IrO_2 improved the activity for OER. $Ir_{0.7}Ru_{0.3}O_2$, while displaying a slightly lower activity than $Ir_{0.9}Sn_{0.1}O_2$, has been claimed to be the most promising electrocatalyst for the OER since no decrease in activity occurs as the RuO_2 content is increased up to 30 mol%. Hence, the interaction of Ir-Ru and the synergetic contribution to the activity are of great interest.

The core-shell nano-catalysts have been widely studied over the past decades in catalysis, biology and energy storage. The activity and catalytic efficiency are directly influenced by the surface composition and stability of the nano-catalysts. For example, Ma *et al.* [86] have employed carbon-supported Ru as the template to prepare $RuO_2@IrO_2$ core-shell nano-catalysts, and the OER specific activity of $RuO_2@IrO_2$ (5.5 μA $cm^{-2}{}_{ox}$) is threefold that of IrO_2 (1.7 μA $cm^{-2}{}_{ox}$) at 1.48 V vs. RHE in 0.5 M H_2SO_4 solution. Li *et al.* [87] have developed the discontinuously covered IrO_2–RuO_2@Ru (the Ir/Ru ratio changes from 1 : 1 to 3 : 1) supported structure, IrO_2–RuO_2@Ru (3 : 1) exhibits the most uniform nanoparticle distribution and the highest activity among all the catalysts, showing an overpotential of only 281 mV at 10 mA cm^{-2}. Meanwhile, excellent durability has been achieved with the overpotential positively shifting by only 16 mV at 10 mA cm^{-2} after 3, 000 cycles through accelerated durability tests (ADTs). Audichon *et al.* synthesized a core-shell-like $IrO_2@RuO_2$ material using a surface modification/precipitation route in an ethanol medium. The crystalline RuO_2 core particles are well covered by IrO_2. Compared with pure IrO_2 or pure RuO_2, the $IrO_2@RuO_2$ displayed the highest accessibility of active sites and showed the promising activity for the OER, owing to an intimate contact between the two oxides in the IrO_2-covered RuO_2 nano-catalysts that collected the RuO_2 intrinsic activity and the IrO_2 stability [88]. N. Danilovic *et al.* found that he Ru-Ir system employed the power of surface segregation to form a nano-segregated “Ir-protective skeleton” that is four times more stable, but equally as active as the commercial real-world Ru-Ir alloy anode catalysts [89]. The activity of oxide materials for the OER is primarily controlled by the stability of surface atoms rather than the energy of adsorption of reaction intermediates.

To improve the active surface area of $Ir_xRu_{1-x}O_2$, the synthesis of $Ir_xRu_{1-x}O_2$-MO_x (M=Sn, Ta, Mo, Co, Ce, Pt. dopant metal) presents to be an effective way [90-100], and nonprecious metal oxides were added to the noble metal mixed oxides. For example, Hutchings *et al.* [90] have demonstrated that a ternary mixed oxide containing SnO_2, RuO_2 and IrO_2 exhibited to be more stable than the catalysts consisting of noble metal oxides only. $Ir_{0.25}Ru_{0.25}Sn_{0.5}O_2$ showed an initially lower activity, but a significantly improved stability which resulted in a superior behavior to that of the IrO_2 and $Ru_{0.5}Ir_{0.5}O_2$ at a testing time of 320 and 730 h. Ir-Ru-Sn ternary oxide-coated electrodes fabricated by thermal decomposition revealed the synergistic/antagonistic effects between the mixed oxides. Marshall *et al.* [91] synthesized the oxide powders of $Ir_xRu_yTa_zO_2$ by an aqueous hydrolysis, followed by thermal oxidation. Remarkable performance has been obtained using the anode materials containing 20-40 mol% Ru and 0-20 mol% Ta. The doped MO_x often has weak catalytic activity and conductivity, high proportion of dopant has been proved to be unavailable [91-95]. Thus, the doped content in $Ir_xRu_{1-x}O_2$-MO_x must be in a highly controlled manner. $Ir_{0.4}Ru_{0.6}Mo_xO_y$ prepared by modified Adams fusion method had a decreased particle size and improved BET surface area without deteriorating the conductivity [96]. Ir and Ru ions at the interface can connect with Mo by the Ir(Ru)-O-Mo bonds around the rutile crystallite, which inhibits the growth of crystallite grains during the fusion process. The single cell with $Ir_{0.4}Ru_{0.6}Mo_xO_y$ (1 A cm^{-2} @1.646 V) shows a higher performance than the cell with $Ir_{0.4}Ru_{0.6}O_2$ (1 A cm^{-2} @1.606 V) without IR-free. The $RuIrCoO_x$ powders were synthesized using a chemical reduction method, followed by thermal oxidation [97]. The single cell with $RuIrCoO_x$ showed a higher performance than the cell with $IrRuO_x$. The cell voltages at 30 mA cm^{-2} are 1.80 and 1.88 V for $RuIrCoO_x$ and $IrRuO_x$.

In the past years, mixed oxides formed by dispersing the noble metal oxide in a more stable nonprecious matrix have been intensively investigated. For instance, binary IrO_2-SnO_2 catalysts are of interest because of the elevated conductivity and stability at high temperatures [47,75,96-112] IrO_2-SnO_2 have been prepared by the Adams fusion [43, 71, 92], sol-gel [101, 104], modified polyol [92, 93], reactive co-sputtering technique [113] and surfactant-assistant methods [102]. The crystal properties of $Ir_xSn_{1-x}O_2$ powders depended on the method used to prepare such materials. Adams fusion method resulted in oxides consisting of at least two separated oxide phases, namely a Sn rich oxide and an Ir rich oxide [92]. In contrast to the commercial Ir black, $Ir_xSn_{1-x}O_2$ (x = 1, 0.67 and 0.52) nanoparticles developed by surfactant-assistant method, present to be amorphous, good dispersion, high pore volume, solid-solution state and Ir-rich surface for bi-metal oxides [102]. Mayousse *et al.* [43] have performed XRD and ICP-AES measurements to highlight that the quantity of Sn was inserted into the oxide lattice in a finely controlled manner. The bulk molar fraction of Sn was introduced in the IrO_2 lattice without phase separation. The crystallinity increased with the addition of SnO_2 [71]. Similar crystal structure and lattice parameters of IrO_2 and SnO_2, and comparable ionic radius of Ir^{4+} (0.077 nm) and Sn^{4+} (0.083 nm) allow the formation a tetragonal $Sn_xIr_{1-x}O_2$ solid solution. A solid solution between iridium and tin oxides with the lattice parameters of the solid solution phase showed a linear relationship over the entire composition range [92, 93, 104]. For example, Ardizzone *et al.* showed that the Ir can substitute Sn in the lattice at any temperature, and the composites obtained at 500 ºC produced the highest stability thanks to their ordered structure [101]. The effect of Sn addition in Ir on the performance of OER is controversial. Marshall *et al.* [92, 93] proved that the electrical resistivity increases as Sn is added to the oxide. There is a significant difference between the materials produced by Adams fusion and the modified polyol method. The former shows twice higher the electrical resistivity than the latter, owing to the difference in structure of the oxides. A lower resistivity could be expected in a solid solution due to a continuous electronic path through oxides. The insulating tin oxide phase in two phase oxide powders reduced the electronic pathway [92]. The addition of tin oxide to iridium oxide particles shows no beneficial effect other than the dilution of more expensive iridium oxide. Pure IrO_2 anodes have the best performance (1.61 V) at 1 A cm^{-2} and 90 ºC [93]. The active area or the number of active sites decreases as the tin content increases. Felix *et al.* showed that $Ir_xSn_{1-x}O_2$ (Sn = 10 mol%) has a significant increase in electrocatalytic activity compared to pure IrO_2 [71]. Li *et al.* showed that the structure of the resulting $Ir_xSn_{1-x}O_2$ samples was strongly related to the Ir/Sn composites [102]. Figure 6 illustrates the strategy of the surfactant-assistant method for the synthesis of $Ir_xSn_{1-x}O_2$ (0 < x < 1) nanoparticles with high Ir contents. $Ir_xSn_{1-x}O_2$ (x = 0.67, 0.52) nanoparticles displayed outstanding activity and stability, owing to the amorphous structure, good dispersion, high pore volume, solid-solution state and Ir-rich surface, relatively large size (10-11 nm) and dissolution of the Sn component (Figure 7). The membrane electrode assembly (MEA) performance using $Ir_{0.52}Sn_{0.48}O_2$ as the anode-metal showed a better performance for 1 A cm^{-2} @1.631 V and 2 A cm^{-2} @1.821 V. Xu *et al.* have observed that at low SnO_2 contents the IrO_2 particles were well dispersed, but at higher SnO_2 contents the active surface area of IrO_2 decreased due to an increase in the average particle size [103].

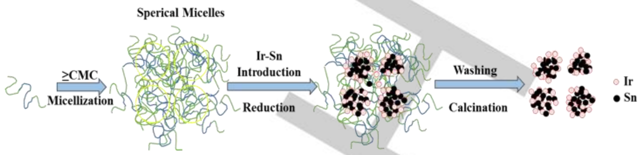

Figure 6. Schematic illustration of the surfactant-assistant method for the fabrication of $Ir_xSn_{1-x}O_2$ (0 < x < 1) NPs with high Ir content. Modified from ref.[102]

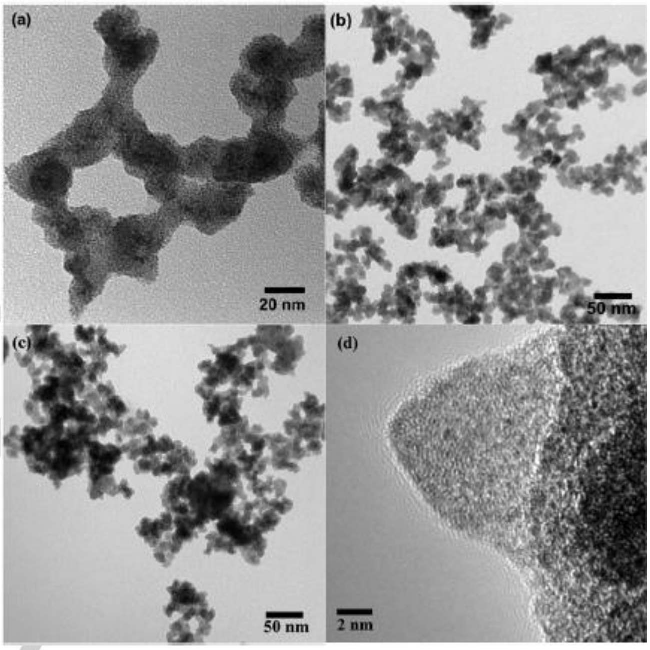

Figure 7. TEM images of (a) as-synthesized $Ir_{0.67}Sn_{0.33}O_2$, (b) IrO_2, (c) $Ir_{0.67}Sn_{0.33}O_2$ and (d) HRTEM image of $Ir_{0.67}Sn_{0.33}O_2$. Reproduced with permission from ref.[102]. Copyright © The Owner Societies 2013.

Ternary Ir-Sn-based mixed oxides have been extensively evaluated as the OER anode electrocatalysts. Pe´rez-Viramontes *et al.* prepared the Ir-Sn-Sb-O by a conventional thermal decomposition method [110]. According to the onset potential for OER tested in 0.5 M H_2SO_4, the Ir-Sn-Sb-O (40) (1.39 V. vs. RHE) electrodes demonstrated a higher activity than the IrO_2/CV (1.45 V vs. RHE) and IrO_2/ATO (1.52 V vs. RHE). The OER kinetics has been improved on the Ir-Sn-Sb-O materials with respect to the mechanical mixture of IrO_2/ATO. The Ir-Sn-Sb-O also presented a higher stability towards OER at an applied potential of 1.55 V vs. RHE than that of the IrO_2 supported on Vulcan carbon. Ternary Sn-Ir-Ta systems have been synthesized by a controlled sol-gel method [111]. In comparison with SnO_2 and binary SnO_2-IrO_2 materials, ternary mixtures presented higher catalytic activities due to that Ta expanded the surface area, improved the electronic conductance and the charge storage capacitance, promotes the surface enrichment of Ir. Kadakia *et al.* synthesized $Ir_{1-2x}Sn_xNb_xO_2$ by thermal decomposition, which was coated on Ti foil [112]. The activity of $(Ir_{0.40}Sn_{0.30}Nb_{0.30})$ O_2 was similar to that of pure IrO_2 with a ~60 mol.% reduction in noble metal content, whereas ($Ir_{0.20}Sn_{0.40}Nb_{0.40}$) O_2 was lower only 20% than pure IrO_2, with a ~80 mol.% reduction in noble metal content, which achieved a remarkable reduction of noble metal oxide loading. Xu *et al.* [114] firstly synthesized Pt activated IrO_2/SnO_2 (2 A cm^{-2} @1.63 V) nano-catalysts for the OER, which showed an enhanced activity than that of IrO_2/SnO_2 (2 A cm^{-2} @1.66 V). This was attributed to the cooperative effects of improved electric conductivity and synergistic effect of Pt and IrO_2/SnO_2, while Pt-IrO_2/SnO_2 showed a short-term stability at 1.52V and 80 ºC in the lab scale single cell setup.

To improve the catalytic activity, a novel dopant/alloying element (F^-) is added to the noble metal oxide electrocatalyst (*e.g.* IrO_2 or RuO_2). F-doped IrO_2 thin film has been studied as a promising oxygen evolution anode electrocatalyst which exhibit a significant improvement in catalytic activity compared to pure IrO_2[115-121]. Kadakia *et al.*[115, 116] synthesized fluorine-doped IrO_2 by thermal decomposition of a homogeneous mixture of $IrCl_4$ and NH_4F dissolved in ethanol-DI water that was solution coated onto pretreated Ti foil, ranging from 0 to 30 wt % of F. The thin film IrO_2: F with 20 wt % F (~11.6 ± 0.1 mA cm^{-2} @1.65V vs.NHE) showed ~19 % higher catalytic activity compared to pure undoped IrO_2 (~9.4 mA cm^{-2} @1.65V vs.NHE) in 1 N H_2SO_4 solution at 40 ºC, which suggested that F-doped IrO_2 could be a promising anode catalyst for OER. They also synthesized (IrO_2: F) powders with varying F contents ranging from 0 to 20 wt% by using modified Adams fusion method [117]. The IrO_2: F with an optimum composition of IrO_2:10 wt% F showed remarkably superior activity and stability compared to pure IrO_2. The IrO_2: F is a solid solution of a single rutile tetragonal structure without any undesirable phase formation like pure IrO_2. This might be due to the similar ionic radius of O^{2-} and F^- being (125 and 120 pm). The molar volume of IrO_2: F of different compositions is comparable to pure IrO_2, indicating that F^- doping in place of O^{2-} has no significant effect on the molar volume of IrO_2: F.

To improve the electrical conductivity of SnO_2, Kanchan *et al.* studied the F doped SnO_2, which had a high corrosion resistance and is electrically conductive. (Sn,Ir)O_2:F containing 10 wt% F showed the same electrochemical activity of IrO_2 (~14±1 mA cm^{-2} @1.55V vs. NHE,40 ºC, 1N H_2SO_4, after iR_Ω correction) with a ~80 mol.% reduction in IrO_2[118, 119].They showed ($Ir_{0.3}Sn_{0.35}Nb_{0.35}$)$O_2$:10wt% F as a promising anode electro-catalyst resulting in ~70 mol.% reduction in IrO_2 content without any compromise in activity, and the current density of ($Ir_{0.3}Sn_{0.35}Nb_{0.35}$)$O_2$:10wt% F at 1.55V(~16 mA cm^{-2} @1.55V vs. NHE) was slightly more than that of pure IrO_2 (~12 mA cm^{-2} @1.55V vs. NHE)(40 ºC, 1N H_2SO_4, after iR_Ω correction)[120]. All of them formed a single phase homogeneous solid solution without any undesirable phase separation. Molar volume of IrO_2: F, (Sn, Ir) O_2: F, and (Ir, Sn, Nb)O_2:x wt.% F is comparable to pure IrO_2, (Sn, Ir)O_2 and (Ir, Sn, Nb)O_2, respectively, indicating that F^- ion substitution/doping has no significant effect on the overall molar volume. This might be due to the comparable ionic radius of O^{2-} (125 pm) to that of F^- (120 pm). Excellent activity exhibited by F^-doped IrO_2 along with the long-term stability make it the appealing anode electrocatalysts for OER in SPE based water electrolysis.

Another approach involved mixing the platinum group metals (PGMs) (Pt[122-124] and Rh[125] with IrO_2. These PGM-oxides are very stable in acidic conditions and very conductive. For example, Ye *et al.*[123] prepared a novel Ti/Pt-IrO_2 electrocatalyst using the dip-coating/calcination method, in which Pt served as a dispersing agent and IrO_2 served as a catalyst. The incorporation of Pt into IrO_2 not only increased the conductivity but also produced a synergic effect to make Pt-IrO_2 much more stable. Seley *et al.*[125] found that the addition of Rh appeared to stabilize and/or enhance the OER activity of IrO_2. Other less expensive and highly corrosion resistant metal oxides including Nb_2O_5 [126-128], Ta_2O_5 [69, 71] in addition to SnO_2 have been explored as proper alternative anode candidates for SPE water electrolysis, which would improve the overall corrosion characteristics of noble metal oxide electro-catalysts, and reduce the cost of noble metal loading. Felix *et al.*[71] synthesized $Ir_xTa_{x-1}O_2$ (1 ≥ x ≥ 0.7) by adapting the Adams fusion method. The addition of Ta_2O_5 to IrO_2 improved the activity, *e.g.,* $Ir_{0.8}Ta_{0.2}O_x$ (~55 mA cm^{-2} @1.6V vs.3M Ag/AgCl electrode) and pure IrO_2 (~35 mA cm^{-2} @1.6V vs.3M Ag/AgCl electrode) (0.5 M H_2SO_4, 25ºC) and suppressed the crystal growth.

2.1.3. Supported catalysts

To reduce the cost of the catalyst, and to enhance the electrocatalytic activity and life-span, one solution is to support electrocatalytic nanoparticles on high specific surface area materials, which will reduce the agglomeration of the electrocatalyst and increase the active surface area. Due to the high over-potential and the corrosive nature of the OER environment, the presence of carbon in the active layer leads to the oxidation of supporting substrate with the following reaction (3), which is not suitable as supports for OER in acidic condition.

$$C+2H_2O \rightarrow CO_2+4H^++4e \quad \text{at 0.206V vs. SHE} \qquad (3)$$

The requirements for a suitable support of the OER electrocatalyst include: 1) high availability and low cost; 2) high stability in the acidic environment; 3) high specific surface area; and 4) good electrical conductivity. The enhanced activity is related to the interaction between the support and the electrocatalyst. Various materials have been applied as supports of Ir including metal oxides such as antimony-doped SnO_2 [129-144], TiO_2 [145-158], titanium suboxide (Ti_nO_{2n-1}) [159-161], or ITO [166, 167], and carbide such as TiC [168, 169], TaC [170, 172], SiC [173] or WC[174-176], due to their corrosion resistance and electrical conductivity.

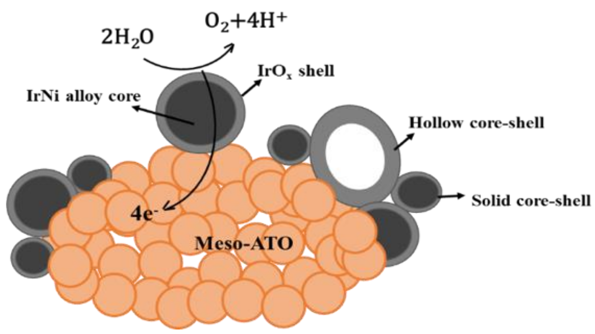

Figure 8. Scheme of the oxygen evolution reaction on the IrO_x shell of $IrNiO_x$ core-shell NPs supported on Meso-ATO. Modified from ref.[136]

Thanks to its good electronic conductivity, availability, high specific surface area and stability at anodic potentials, ATO has been widely used as the supports for the OER [129-144]. The performance of ATO supported Pt or RuO_2 was better than that of pristine Pt/C or RuO_2[129, 130]. The Pt/ATO catalyst possessed a ~90% of the origin catalytic activity after 3, 000 cycles, while the Pt/C was ~36%. With the same amount of RuO_2, RuO_2/ATO exhibited higher voltammetric charge than unsupported RuO_2. This was attributed to the lower agglomeration of active crystallites on the ATO. The effects of various parameters such as particle size, electronic conductivity and specific surface area on the performance of the ATO supported IrO_2 catalysts were systematically investigated. Marshall *et al.* studied a bimetallic IrO_2-RuO_2 supported on commercial ATO nanoparticles with various loading levels (5, 10 and 20 wt.%) [131]. The electrochemically active surface area of 75 mol% IrO_2-25 mol% RuO_2 clusters is maximized, the electrochemically active surface area decreased with decreasing the loading of IrO_2-RuO_2 on ATO, and 20 wt% $Ru_{0.25}Ir0_{.75}O_2$ on ATO presented the highest activity in aqueous 0.5 M H_2SO_4. Puthiyapura *et al.* achieved a 40 wt% reduction in the IrO_2 by utilizing ATO as support materials [133]. The membrane–electrode assembly (MEA) performance showed a better performance for 60 wt% IrO_2-ATO (1625 mA cm^{-2} @1.8 V) than that of the pristine IrO_2 (1341 mA cm^{-2} @1.8 V) under the same conditions that the MEA used Nafion-115 membrane at 80 ºC and atmospheric pressure. The higher performance of 60 wt% IrO_2-ATO was mainly attributed to a better dispersion of active IrO_2 on the electrochemically inactive ATO support materials, the formed smaller IrO_2 crystallites, a continuous electronic network, higher BET surface area and similar conductivity to that of pristine IrO_2. Oh *et al.*[59, 134-137] studied that the mesoporous Sb-doped tin oxides synthesized through TDA soft-template method as the supports were highly stable compared to carbon black due to their mesoporous structure, small particle size, high specific surface area and electrical conductivity. The Ir-ND/ATO catalyst displayed a more than 2-fold larger kinetic water splitting activity compared with IrO_x/C and 8-fold larger catalytic mass-based activity than commercial Ir blacks [59]. The metal/metal-oxide support interactions (MMOSI) play a critical role in the performance of Ir acid water splitting catalysts [137]. In a higher current density of 10 mA cm^{-2}, the measured potential sharply increased to 2.4 V_{RHE} after 15 min and 1.2 h for IrO_x/C (Vulcan XC-72R, Cabot, 235 m^2 g^{-1}) and IrO_x/Com. ATO (commercial ATO, SnO_2/Sb_2O, ≥99.5%, Sigma-Aldrich, 47 m^2 g^{-1}), respectively, whereas the IrO_x/ATO catalyst showed a negligible degradation during the stability test, even though their working potentials were initially similar. After the stability test, the Ir mass loss of IrO_x/ATO was 28.3% of their initial Ir loading, while IrO_x/C was 97.1%, which suggested that the metal/metal-oxide support interactions (MMOSI) helped to maintain a higher IrO_x loading and thus sustained a higher charge-transfer kinetics. The Meso-ATO powder has a higher specific surface area (264 m^2 g^{-1}) than commercial ATO. Nong *et al.* [136] presented a novel catalyst/support couple concept--an electrochemically dealloyed IrNi core IrO_x shell concept combined with a mesoporous corrosion-resistant oxide support. The $IrNiO_x$ core-shell structure has been obtained from IrNi nanoparticle precursor alloys using electrochemical selective dealloying of Ni and a simultaneous surface oxidation of the surface Ir atoms resulting in IrOx shells. $IrNiO_x$/Meso-ATO core-shell material (~90 A g^{-1}_{Ir}) showed a 2.5 times higher Ir-mass-based activity compared to IrOx/C (Vulcan XC-72R, ~250 m^2 g^{-1}) (~40 A g^{-1}_{Ir}) and IrOx/com.-ATO (Sigma Aldrich, 47 m^2 g^{-1}) (~35 A g^{-1}_{Ir}) at an overpotential η=280 mV vs.RHE in 0.05 M H_2SO_4. Figure 8 illustrates the structure hypothesis regarding the active catalyst/support couple. With thin IrO_x shells on the Ir-low/Ir-free cores, the proceeding OER reduced the Ir amount significantly. Wang *et al.*[141] prepared a novel Ir supported on a SnO_2:Sb aerogel OER catalyst (Ir/SnO_2:Sb-mod-V), which allowed a decrease of more than 70 wt% for precious metal usage in the catalyst layer while keeping a similar OER activity compared to its unsupported counterpart.

TiO_2 is an option because of its high resistance against anodic corrosion and controllable morphology. Since TiO_2 itself typically shows insulating properties, electrocatalysts must be introduced into the TiO_2 by coating or doping. For example, Mazu´r *et al.* studied the electrocatalysts IrO_2/TiO_2 with three TiO_2 samples at different specific surface areas, *i.e.,* R200M (10 m^2 g^{-1}), P25 (50 m^2 g^{-1}), P90 (90 m^2 g^{-1}) [145]. The lower the specific surface area of the TiO_2 supports, the higher the activity of the catalyst, due to the formation of a conductive IrO_2 film on the surface of non-conductive supports. Oakton *et al.* developed a high specific surface area IrO_2-TiO_2 with chlorine-free, which was a highly active and stable OER catalyst in acidic media [146]. 40 mol % IrO_2-TiO_2 improved the OER activity and stability compared to the benchmark catalyst. The presence of iridium hydroxo surface species was associated with the high OER activity. Lu *et al.* [147] have revealed that IrO_2/H-TNTA reached 5-fold higher current density at 1.6 V vs. RHE in 0.5 M H_2SO_4 solution than IrO_2/air-TNTA with the improved conductivity. Conductive suboxides of titanium, such as Ebonex®, have been studied as electroactive materials. Siracusano *et al.* prepared titanium suboxides with Magneli phase as the conductive supports of IrO_2[159]. As a result, IrO_2 based on the Ti-suboxides exhibited a larger voltammetric charge and double layer capacitance compared to the anode based on the commercial support, owing to a better dispersion and larger occurrence of active catalytic sites on the surface of the suboxide [160,161]. TiO_2 doped with Nb [162-164] and V [165] has been reported to achieve considerable conductivity and high stability. Hao *et al.* [162] found that IrO_2/TN-20(20 at.% Nb) possessed the highest OER activity (2.027 V @1 A cm^{-2}) superior to that of pristine IrO_2/TiO_2 (2.218 V @1 A cm^{-2}) in single-cell tests at 80 ºC. The increase in OER activity originated from the Nb-doping that restricted the crystal structure to a single phase of anatase and induced the enhancement of the specific surface area and activity of transferring charge and species. The additional redox couples of Nb(IV)/Nb(V) accounted for this enhancement. Xia *et al.* studied $IrO_2/Nb_{0.05}Ti_{0.95}O_2$ (26 wt%) and revealed the best mass-based activity at 1.6 V_{RHE} (471 A g IrO_2^{-1}) in 0.5M H_2SO_4 [163], which was 2.4-fold larger than that of unsupported IrO_2 (198 A g IrO_2^{-1}). Hao *et al.* found the 40Ir/TV-20 (titania doped by 20 at.% V) emerged as the best V-doped titania support for IrO_2 catalyst (2.015 V@1 A cm^{-2}, 80 ºC) [165] . The V dopant on titania supports enhanced the simplification of phase composition and consequently improved the homogeneity of porous morphology, and introduced redox couple V (IV)/V (V) to the surface of titania. Other materials such as ITO [166, 167], TiC [51, 168, 169], TaC [170, 172], Ta_2O_5 [171], WC, WO_3 [174-176] and RGO [177] were also studied as support materials for anode catalysts. Puthiyapura *et al.* have picked ITO as support because of the remarkable thermal stability of ITO [166]. The 90 % IrO_2-ITO produced a similar performance (1.74 V@1 A cm^{-2}) to that of the unsupported IrO_2 (1.73 V@1 A cm^{-2}) at the same working conditions (MEA polarisation test at 80 ºC with Nafion 115 membrane). Peter *et al.* prepared thin Ir film on TiC-based support sublayer by magnetron sputtered [51]. The supported Ir/TiC catalysts had a higher stability than pristine Ir, which was in good agreement with the findings by Sui *et al.* [168] and Ma *et al.* [169]. WC and WO_3 have been chosen as support [174], and the optimal route of WO_3/WC supported $Ir_{0.5}Ru_{0.5}O_2$ catalysts was mechanical mixing of support and catalyst followed by annealing under inert atmosphere. Kong *et al.* [177] have proved that the catalytic activity of IrO_2/RGO (1.65 V vs.RHE@5.01 A mg^{-1}) hybrid towards OER was 2.3 times that of commercial IrO_2 (1.65 V vs.RHE @2.19A mg^{-1}) in the OER polarization curves in 0.5 M H_2SO_4 solution at 25 ºC. These were attributed to a better dispersion of active IrO_2 on the electrochemically inactive support, giving rise to smaller catalyst particles and thereby a higher specific surface area. All the supported catalysts showed a higher efficiency of utilization of the precious metal than pure IrO_2. The conductivity of the support is not significant when there is enough concentration of a highly conductive active part. This suggests that these oxides may be of economic advantage to use as SPE water electrolysis anodes.

2.1.4 Structural modification of iridium oxides

Nanoparticulated materials efficiently dispersed on a support, highly porous layers, core-shell and mixed oxide systems have been suggested to reduce the loading of expensive elements.[178-183] An alternative way is the structural modification of iridium oxides. Extensive efforts have been devoted to resolving the structure−property relationship.[184-200]

Recent development of techniques for high-quality growth of epitaxial complex oxide thin films and heterostructures provides an intriguing opportunity for the conception and fundamental study of OER catalysts [184, 185]. For example, Viktoriia *et al.* developed a nanostructured iridium catalyst after electrochemically leaching ruthenium from metallic iridium-ruthenium [184], *i.e.,* $Ir_{0.7}Ru_{0.3}O_x$ (EC). The dissolution of unstable Ru led to an unparalleled OER activity of the remaining Ir-rich catalyst compared to the classic thermally treated $Ir_{0.7}Ru_{0.3}O_2$ (TT). $Ir_{0.7}Ru_{0.3}O_x$ (EC) (1.68 V@1 A cm^{-2}) showed an unparalleled 13-fold higher OER activity compared to the $Ir_{0.7}Ru_{0.3}O_2$ (TT) (1.73 V@1 A cm^{-2}), proving that $Ir_{0.7}Ru_{0.3}O_x$ (EC) was one of the most efficient anodes to date. Linsey *et al.* reported an iridium oxide/strontium iridium oxide (IrO_x/$SrIrO_3$) catalyst which was formed during the electrochemical testing by strontium leaching from surface layers of thin films of $SrIrO_3$ [185]. The IrO_x/$SrIrO_3$ outperformed the well-known IrO_x and RuO_x systems. Density functional theory (DFT) calculations suggested the formation of highly active surface layers during the strontium leaching with IrO_3 or anatase IrO_2 motifs. They pinpointed that the surface IrO_x formed by means of the in-situ leaching process of Sr from $SrIrO_3$ is more active than the deposited IrO_x. Figure 9 shows the AFM maps and line scans for a 100 nm $SrIrO_3$ film before and after 30-hour OER testing. Although there was some surface rearrangement, the films exhibited uniform small features after stability testing. The stability and high intrinsic activity of this catalyst show promise for its integration into renewable energy technologies, such as PEM electrolyzers, for the sustainable production of hydrogen or other fuels and chemicals.

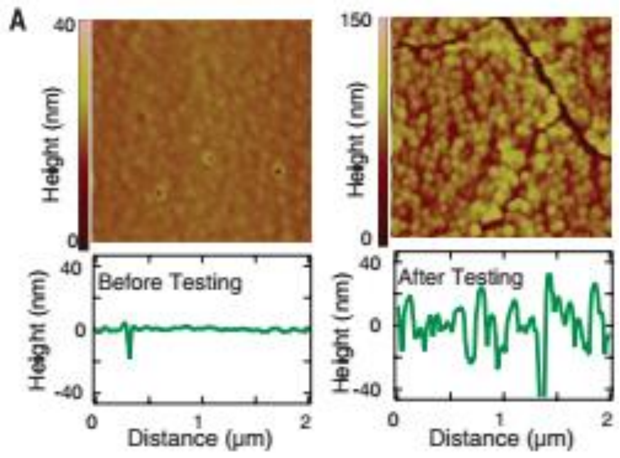

Figure 9. AFM maps and line scans for a 100-nm $SrIrO_3$ film before and after 30 hours of OER testing. Reproduced with permission from ref. [185]. Copyright © The sciencemag.org Science 2016.

In addition, the most prominent examples are iridium-based perovskites recently investigated in acidic electrolyte [185-190]. Grimaud, A. *et al.* [189], used La_2LiIrO_6 as a model catalyst, provided that the OER activity for Ir- or Ru-based oxides is often associated with surface instability. This correlation is rooted in the activation of surface oxygen, leading to the modification of the Ir coordination. Perovskites show high dissolution in the range of amorphous/hydrous oxide and therefore might not be suitable for long-term operation. Similar structures can be achieved by leaching Sr from $SrIrO_3$ or Ni from IrNiOx[185, 187].The case study on iridium-based perovskites showed that leaching of the non-noble elements in mixed oxides results in the formation of highly active amorphous iridium oxide, the instability of which is explained by the generation of short-lived vacancies that favour dissolution. The participation of activated lattice oxygen atoms as a trigger for enhancing activity and the high dissolution rate due to the arising oxygen vacancies. The activity is not related to the chosen rare earth element, but rather to the amorphous structure that forms after leaching. These insights drove the further research to be devoted to increasing the utilization of highly durable pure crystalline iridium oxide and finding solutions to stabilize amorphous iridium oxides.

Iridium, amongst other metals, is able to form an amorphous hydrous oxide under continuous potential cycling. In these studies [191-193], it emphasized the key role of amorphous Ir oxohydroxides in high current, stable OER electrocatalysis in contrast to the less active crystalline IrO_2. Pfeifer et al.[195, 196] investigated the electronic structure of active Ir oxide-based catalysts and confirmed the higher OER performance of amorphous IrIII/IV oxohydroxides in comparison with IrO_2. The superior intrinsic activity of these materials was relevant to the ability to accommodate nucleophilic reactive oxygen species.[197] Willinger et al.[199] concluded that the ratio between corner- and edge-sharing IrO_6 octahedra is determining the OER activity. Thus, a high number of corner-sharing oxygen atoms (activated oxygen) facilitates the OER. They also identified the key hollandite-like structural motifs that are associated with high catalytic activity and stability in OER. Massue et al. [200] synthesized a novel Ir oxohydroxides by rapid microwave-asisted hydrothermal synthesis, which bridges the gap between electrodeposited amorphous IrO_x films and crystalline IrO_2 electrocatalysts prepared by calcination routes.In addition, K^+ cation has a great influence on the performance of the catalyst. The residual presence of K ions in the IrO_x-FHI (IrO_x hydroxide synthesized at the Department of Inorganic Chemistry of the Fritz Haber Institute) catalyst might play an important role in catalytic stability, as it stabilizes the hollandite-like open framework structure.[199] K^+ cations present in smaller amounts in the Ir oxohydroxides obtained for KOH/Ir,5:1 play a major role in stabilizing a high-performance Ir oxohydroxide phase containing high amounts of OER-relevant hydroxyl groups. These studies provided several important clues on the structural features determining the OER performance of Ir oxohydroxides. [201][202]

3. Conclusions and Perspectives

Water is the most renewable resource of sustainable hydrogen in the future. Water electrolysis is the important production method, and based on this technology, hydrogen has a high purity that can reach 99.999 vol.% by drying up and removing oxygen impurities. SPE water electrolysis has more advantages in comparison to the traditional alkaline water electrolysis, which includes small size and mass, low gas crossover and power consumption, high proton conductivity, high pressure operation, and higher safety level. For SPE electrolyzers, the current efficiency has reached as high as 99%. The main disadvantages of SPE water electrolysis are the slow kinetics, which is one of the largest sources of cell efficiency loss of OER. The development of active and stable OER catalysts has been extensively investigated [202]. The material composition and morphology have an impact on the catalyst activity toward the OER and corrosion stability. With the increase of temperatures, the crystallite size and crystallinity increase, the crystal specific surface area decreases, and the electrocatalytic activity decreases.

There are two main strategies to improve the activity of an electrocatalyst. One is to increase the number of active sites on a given electrode, such as alloying or doping some inexpensive metals in the iridium catalyst or to support nanoparticles on high surface area materials, which can change the electronic and structural properties and improve the activity and stability. Supported catalysts can significantly increase the dispersion of the active phase, provide high specific surface area and enough active sites for OER. The other method is to increase the intrinsic activity of each active site, which can be achieved by the introduction of defects.

Many studies have been conducted on methods and materials for the anodes of SPE water electrolysis, but the situation remains challenging. To date, no credible alternative to IrO_2 has been reported. Hence, substantial research and development efforts are needed to elucidate the details of the electrode-electrolyte interface in theory and experiments. The development of both experimental and computational methods is an important frontier that can precisely unravel the reaction mechanisms on catalyst materials and in harsh operating conditions. An appropriate theoretical model incorporating the kinetics at the electrode's surfaces and transport in the membrane should be established to analyze the current-potential characteristics of SPE water electrolysis cell based on the involved charge and mass balances. Useful information will pave the way for the development of high activity and stability of OER catalysts.

Acknowledgements

Financial support was provided by the National Natural Science Foundation of China (Project No. 51503187, 21504037 and 51603194); the National key R&D Project (Project No. 2016YFE0102700); the Shanxi provincial foundation for science and technology research (Project No. 201601D021058, 201701D221050, 20181101006, 20181102019). Partial support is also from the NIMHD-RCMI grant number 5G12MD007595 from the National Institute of Minority Health, Health Disparities and the NIGMS-BUILD grant number 8UL1GM118967 and National Science Foundation (Grant 1700429). Q. Gao was supported as part of the Fluid Interface Reactions, Structures and Transport (FIRST) Center, an Energy Frontier Research Center funded by the U.S. Department of Energy, Office of Science, Office of Basic Energy Sciences. A portion of this work was conducted at the Center for Nanophase Materials Sciences, which is a DOE Office of Science User Facility.

Keywords: Solid polymer electrolytes • water electrolysis • oxygen evolution • electrocatalyst

[1] Z. W. Seh, J. Kibsgaard, C. F. Dickens, I. Chorkendorff, J. K. Nørskov and T. F. Jaramillo, Science, **2017**, 355, eaad4998;
[2] N. S. Lewis, Science, **2016**, 351, aad1920;
[3] F. Barbir, Sol. Energy, **2005**, 78, 661-669;
[4] Carmo. M., Fritz. D. L., Mergel. J., Stolten. D, Int. J. Hydrogen Energy, **2013**, 38, 4901-4934;
[5] Wang. M, Wang. Z, Gong. X, Guo. Z, Renewable Sustainable Energy Rev, **2014**, 29, 573-588;
[6] A. Marshall, B. Børresen, G. Hagen, M. Tsypkin, R. Tunold, Energy, **2007**, 32, 431-436;
[7] A. S. Arico`, S. Siracusano, N. Briguglio, V. Baglio, A. Di Blasi and V. Antonucci, J Appl Electrochem, **2013**, 43, 107-118;
[8] A. Ursu´a, L. M. Gandı´a and P. Sanchis, Proceedings of the IEEE, **2012**, 100, 410-426;
[9] P. Millet, Compendium of Hydrogen Energy, **2015**.
[10] D. Tyagi, K. Scholz, S. Varma, K. Bhattacharya, S. Mali, P.S. Patil and S.R. Bharadwaj, Int. J. Hydrogen Energy, **2012**, 37, 3602-3611;
[11] B.-S. Lee, H.-Y. Park, I. Choi, M. K. Cho, H.-J. Kim, S. J. Yoo, D. Henkensmeier, J. Y. Kim, S. W. Nam, S. Park, K.-Y. Lee and J. H. Jang, J. Power Sources, **2016**, 309, 127-134;
[12] Grigoriev, S. A, Millet. P, Fateev. V. N, J. Power Sources, **2008**, 177, 281-285;
[13] Xu, G.-R., Hui, J.-J., Huang, T., Chen, Y., Lee, J.-M. J. Power Sources, **2015**, 285, 393-399;
[14] Yang. T, Du. M, Zhu. H, Zhang. M, Zou. M, Electrochim. Acta, **2015**, 167, 48-54;
[15] S.A. Grigoriev, M.S. Mamat, K.A. Dzhus, G.S. Walker and P. Millet, Int. J. Hydrogen Energy, **2011**, 36, 4143-4147;
[16] A. Stoyanova, G. Borisov, E. Lefterova and E. Slavcheva, Int. J. Hydrogen Energy, **2012**, 37, 16515-16521;
[17] Matsumoto. Y, Sato, E. Electrocatalytic Properties of Transition Metal Oxides for Oxygen Evolution Reaction. Mater. Chem. Phys. **1986**, 14, 397-426;
[18] E. Fabbri,* A. Habereder, K. Waltar, R. Kötz and T. J. Schmidt. Catal. Sci. Technol, **2014**, 4, 3800-3821;

[19] J. M. Hu, J. Q. Zhang, J. M. Wang. C. N. Cao, Functional Materials, **2002**, 33, 363-366;
[20] S. Trasatti, J. Electroanal. Chem, **1980**, 111, 125-131;
[21] S. Trasatti, Electrochim. Acta, **1984**, 29, 1503-1512;
[22] C. C. McCrory, S. Jung, I. M. Ferrer, S. M. Chatman, J. C.Peters and T. F. Jaramillo, J. Am. Chem. Soc, **2015**, 137,4347-4357;
[23] M. Huynh, D. K. Bediako and D. G. Nocera, J. Am. Chem.Soc, **2014**, 136, 6002-6010;
[24] N. Danilovic, R. Subbaraman, K. C. Chang, S. H. Chang, Y. J. Kang, J. Snyder, A. P. Paulikas, D. Strmcnik, Y. T. Kim, D. Myers, V. R. Stamenkovic and N. M. Markovic, J. Phys. Chem. Lett, **2014**, 5, 2474-2478;
[25] Elisa A. Paoli, et al. Chemical Science, **2015**, 6, 190-196;
[26] N. Hodnik, P. Jovanovic, A. Pavlisic, B. Jozinović, M. Zorko, M. Bele, V. S. Šelh, M. Šala, S. Hocevar and M. Gabersč ek, J. Phys. Chem. C, **2015**, 119, 10140-10147;
[27] S. Cherevko, S. Geiger, O. Kasian , N. Kulyk , J.-P. Grote, A. Savan, B. R. Shrestha, S. Merzlikin , B. Breitbach, A. Ludwig and K. J.J. Mayrhofer, Catal Today, **2016**, 262, 170-180;
[28] J.M. Eugene, O. Sullivan, J.R. White, J. Electrochem. Soc., **1989**, 136, 2576-2583;
[29] A. Damjanovic, A. Dey and J. O. M. Bockris, J. Electrochem. Soc, **1966**, 113, 739-746;
[30] Youngmin Lee,Jin Suntivich, Kevin J. May, Erin E. Perry, Yang Shao-Horn. J. Phys. Chem. Lett. **2012**, 3, 399-404;
[31] P. C. K. Vesborg and T. F. Jaramillo, RSC Adv., **2012**, 2, 7933-7947;
[32] J.-M. Hu, J.-Q. Zhang and C.-N. Cao, Int. J. Hydrogen Energy, **2004**, 29, 791-797;
[33] S.A. Grigoriev, A.A. Kalinnikov. Int. J. Hydrogen Energy, **2017**,42, 1590-1597;
[34] Grigoriev SA, Millet P, Dzhus KA, Middleton H, Saetre TO, Fateev VN. Int J Hydrogen Energy May **2010**, 35, 5070-5076;
[35] Caroline Rozain, Eric Mayousse, Nicolas Guillet , Pierre Millet . Applied Catalysis B: Environmental, **2016**, 182, 153-160;
[36] Serhiy Cherevko, Tobias Reier, Aleksandar R. Zeradjanin, Zarina Pawolek, Peter Strasser, Karl J.J.Mayrhofer. Electrochemistry Communications, **2014**, 48, 81-85;
[37] Fierro, S.; Kapałka, A.; Comninellis, C. Electrochem. Commun. **2010**, 12, 172-174;
[38] Anita Skulimowska, Marc Dupont, Marta Zaton, Svein Sunde, Luca Merlo, Deborah J. Jones, Jacques Rozie`re. Int. J. Hydrogen Energy, **2014**, 39, 6307-6316;
[39] Guoqiang Wei, Yuxin Wang, Chengde Huang, Qijun Gao, Zhitao Wang, Li Xu. Int. J. Hydrogen Energy, **2010**, 35, 3951-3957;
[40] E. Rasten, G. Hagen and R. Tunold, Electrochim. Acta, 2003, 48, 3945-3952;
[41] D. F. Abbott, D. Lebedev, K. Waltar, M. Povia, M. Nachtegaal, E. Fabbri, C. Coperet and T. J. Schmidt, Chem. Mater. **2016**, 28, 6591-6604;
[42] S.D. Song, H.M. Zhang, X.P. Ma, Z.G. Shao, R. T. Baker and B.L. Yi, Int. J. Hydrogen Energy, **2008**, 33, 4955-4961;
[43] E. Mayousse, F. Maillard, F. F.-Onana, O. Sicardy and N. Guillet, Int. J. Hydrogen Energy, **2011**, 36, 10474-10481;
[44] J. Xu, M. Wang, G. Liu, J. Li, X. Wang, Electrochim. Acta, **2011**, 56, 10223-10230;
[45] C. Felix, T. Maiyalagan, S. Pasupathi, B. Bladergroen, V. Linkov, Micro. Nanosystems, **2012**, 4, 186;
[46] J. C. Cruz, V. Baglio, S. Siracusano,R. Ornelas, L. Ortiz-Frade, L. G. Arriaga, V. Antonucci, A. S. Arico. J. Nanopart Res, **2011**, 13, 1639-1646;
[47] J. C. Cruz, V. Baglio, S. Siracusano V. Antonucci, A. S. Aricò, R. Ornelas, L. Ortiz-Frade, G. Osorio-Monreal, S. M. Durón-Torres, L.G. Arriaga. Int. J. Electrochem Sci, **2011**, 6, 6607-6619;
[48] S. Siracusano, V. Baglio, A. Stassi, R. Ornelas, V. Antonucci and A.S. Arico, Int. J. Hydrogen Energy **2011**, 36, 7822-7831;
[49] E. Slavcheva, I. Radev, S. Bliznakov, G. Topalov, P. Andreev, E. Budevski, Electrochim. Acta, **2007**, 52, 3889-3894;
[50] L. Ouattara, S. Fierro, O. Frey, M. Koudelka and C. Comninellis, J Appl Electrochem, **2009**, 39, 1361-1367;
[51] P. Kus, A. Ostroverkh, K. Sevikova, I. Khalakhan, R. Fiala, T. Skala, N. Tsud and V. Matolin, Int. J. Hydrogen Energy, **2016**, 41, 15124-15132;
[52] P. Lettenmeier, J. Majchel, L. Wang, V. A. Saveleva, S. Zafeiratos, E. R. Savinova, J.-J. Gallet, F. Bournel, A. S. Gago and K. A. Friedrich. Chem. Sci, **2018**, 9, 3570-3579;
[53] M. Sapountzi, S.C. Divane, E.I. Papaioannou, S. Souentie, C.G. Vayenas. Journal of Electroanalytical Chemistry, **2011**, 662, 116-122;
[54] Byung-Seok Lee , Sang Hyun Ahn , Hee-Young Park , Insoo Choi , Sung Jong Yoo ,Hyoung-Juhn Kim , Dirk Henkensmeier , Jin Young Kim , Sehkyu Park ,Suk Woo Nam , Kwan-Young Lee , Jong Hyun Jang. Applied Catalysis B: Environmental, **2015,** 179, 285-291;
[55] G.Q. Li, S.T. Li, M.L. Xiao, J.J. Ge, C.P. Liu, W. Xing, Nanoscale, **2017**, 9, 9291-9298;
[56] E. Ortel, T. Reier, P. Strasser and R. Kraehnert, Chem. Mater. **2011**, 23, 3201-3209;
[57] G.F. Li, H.M. Yu, W. Song, M.L. Dou, Y.K. Li, Z.G. Shao and B.L. Yi, ChemSusChem, **2012**, 5, 858;
[58] W. H. Lee, H. Kim, Catalysis Communications, **2011**, 12, 408-411;
[59] H.-S. Oh, H. N. Nong, T. Reier, M. Gliech and P. Strasser, Chem. Sci., **2015**, 6, 3321-3328;
[60] Y. Pi, N. Zhang, S. Guo, J. Guo and X. Huang, Nano Lett, **2016**, 16, 4424-4430;
[61] C. Zhao, H. Yu, Y. Li, X. Li , L. Ding, L. Fan. Journal of Electroanalytical Chemistry, **2013**, 688, 269-274;
[62] Y.-T. Kim, P. P. Lopes, S.-A. Park, A-Y. Lee, J. Lim, H. Lee, S. Back, Y. Jung , N. Danilovic, V. Stamenkovic, J. Erlebacher, J. Snyder, N. M. Markovic. Nature Communications 2017, 8 (1), 1449.
[63] P. P. Patel, M. K. Datta, O. I. Velikokhatnyi, R. Kuruba, K. Damodaran, P. Jampani, B. Gattu, P. M. Shanthi, S. S. Damle and P. N. Kumta, Sci. Rep, **2016**, 6, 28367-28380;
[64] J. Roller, J. A. Jiménez, R. Jain, H. Yu, R. Maric and C.B. Carter, J. Electrochem. Soc, **2013**, 45, 97;
[65] J. M. Roller, M. J. Arellano-Jimenez, R. Jain, H. Yu, C. B. Carter and R. Maric, J. Electrochem. Soc, **2013**, 160, F716-F730;
[66] T. Audichona, N. Mamacaa, C. Moraisa, K. Servata, T.W. Napporna, E. Mayousseb, N. Guilletb, K.B. Kokoha, ECS Transactions, 2013, 45, 47-58 ;
[67] N. Mamaca, E. Mayousse, S. Arrii-Clacens, T.W. Napporn, K. Servat, N. Guillet and K.B. Kokoh. Applied Catalysis B: Environmental, **2012**, 111-112, 376-380;
[68] L. E. Owe, M. Tsypkin, K. S. Wallwork, R. G. Haverkamp, S. Sunde, Electrochim. Acta, **2012**, 70, 158-164;
[69] A. Di Blasi, C. D'Urso, V. Baglio , V. Antonucci, A. S. Arico' , R. Ornelas, F. Matteucci , G. Orozco ,D. Beltran, Y. Meas and L. G. Arriaga, J Appl Electrochem, **2009**, 39, 191-196;
[70] J.B. Cheng, H.M. Zhang, G.B. Chen, Y.M. Zhang. Electrochim. Acta **2009**, 54, 6250-6256;
[71] C. Felix, T. Maiyalagan, S. Pasupathi, B. Bladergroen and V. Linkov, Int. J. Electrochem. Sci, **2012**, 7, 12064-12077;
[72] S. Siracusano , N. Van Dijk , E. Payne-Johnson , V. Baglio , A.S. Aricò, Applied Catalysis B: Environmental, **2015**, 164, 488-495;
[73] Kötz, R.; Stucki, S. Electrochim. Acta **1986**, 31, 1311-1316;
[74] Lodi, G.; Sivieri, E.; Battisti, A.; Trasatti, S. J. Appl. Electrochem. **1978**, 8, 135-143;
[75] F. I. Mattos-Costa, P. de Lima-Neto, S. A. S. Machadoa, L. A. Avaca, Electrochim. Acta. **1998**, 44, 1515-1523;
[76] C. Angelinetta, S. Trasatti, L. D. Atanasoska, Z. S. Minevski, R. T. Atanasoski, Mater. Chem. Phys. **1989**, 22, 231-247;
[77] S. Siracusano, V. Baglio, E. Moukheiber , L. Merlo b, A.S. Arico. Int. J. Hydrogen Energy, **2015**, 40, 14430-14435;
[78] F. Hegge, R. Moroni, P. Trinke, B. Bensmann, R. H.-Rauschenbach, S. Thiele, S. Vierrath. J. Power Sources, **2018**, 393, 62-66;
[79] Stefania Siracusano, Vincenzo Baglio, Nicholas Van Dijk, Luca Merlo, Antonino Salvatore Aricò. Appl. Energy, **2017**, 192, 477-489;
[80] Y. Murakami, S. Tsuchiya, K. Yahikozawa, Y. Takasu, J. Mater. Sci. Lett. **1994**, 13, 1773-1774;

10.1002/cssc.201802873

[81] M. Ito, Y. Murakami, H. Kaji, H. Ohkawauch, K. Yahikozawa, Y. Takasu, J. Electrochem. Soc, **1994**, 141, 1243-1245;

[82] N. Danilovic, R. Subbaraman, K. C. Chang, S. H. Chang, Y. Kang, J. Snyder, A. P. Paulikas, D. Strmcnik, Y. T. Kim, D. Myers, V. R. Stamenkovic, N. M. Markovic, Angew. Chem., Int. Ed. **2014**, 53, 14016-14021;

[83] T. Audichon, E. Mayousse, S. Morisset, C. Morais, C. Comminges, T. W. Napporn, K. B. Kokoh, Int. J. Hydrogen Energy **2014**, 39, 16785-16796;

[84] O. Kasian, S. Geiger, P. Stock, G. Polymeros, B. Breitbach, A. Savan, A. Ludwig, S. Cherevko, and K. J. J. Mayrhofer, J. Electrochem. Soc., **2016**, 163, F3099-F3104;

[85] V. A. Saveleva, L. Wang, W. Luo, S. Zafeiratos, C. U.-Bouillet, A. S. Gago, K. A. Friedrich and E R. Savinova, J. Phys. Chem. Lett, **2016**, 7, 3240-3245;

[86] M. Zhong, Y. Zhang, S Liu, W Xu, L Wu, Y Hsieh, P Liu, Y Zhu, K Sasaki, Julie N. Renner, Katherine E. Ayers, Radoslav R. Adzic, Jia X. Wang. J. Electroanalytical Chem., **2018**, 819, 296-305;

[87] G Li, S Li, J Ge, C Liu, W Xing. J. Mater. Chem. A, **2017**, 5, 17221-17229;

[88] T. Audichon, Teko W. Napporn, C Canaff, C Morais, C Comminges, ´K. Boniface Kokoh. J. Phys. Chem. C, **2016**, 120, 2562-2573;

[89] N. Danilovic, R. Subbaraman, K. C. Chang, S. H. Chang, Y. Kang, J. Snyder, A. Paul P., D. Strmcnik, Y. T. Kim, D. Myers, V. R. Stamenkovic, and N. M. Markovic.. Angew. Chem. Int. Ed. 2014, 53, 14016 –14021.

[90] R. Hutchings, K. Müller, Kötz and S.Stucki, J. Mater. Sci., **1984**, 19, 3987-3994;

[91] A. T. Marshall, S. Sunde, M. Tsypkin and R. Tunold, Int. J. Hydrogen Energy, **2007**, 32, 2320-2324;

[92] A. Marshall, B. Børresen, G. Hagen, M. Tsypkin and R. Tunold, Mater Chem Phys, **2005**, 94, 226-232;

[93] A. Marshall, B. Børresen, G. Hagen, M. Tsypkin and R. Tunold, Electrochim Acta, **2006**, 51, 3161-3167;

[94] S. Lin, T. Wen. J. Electrochem. Soc., **1993**, 140, 2265-2271;

[95] K. Kameyama, K. Tsukada, K. Yahikozawa K, Y. Takasu , J. Electrochem. Soc., **1994**, 141, 643-647;

[96] J. Cheng, H. Zhang, H. Ma, H. Zhong, Y. Zou, Int. J. Hydrogen Energy, **2009**, 34, 6609-6613;

[97] J. Corona-Guinto, L. Cardeno-Garcia, D.C. Martinez-Casillas, J.M. Sandoval-Pineda, P. Tamayo-Meza , R. Silva-Casarin and R.G. Gonzalez-Huerta. Int. J. Hydrogen Energy, **2013**, 38, 12667-12673;

[98] T. Audichon, S. Morisset, T. W. Napporn, K. B. Kokoh, C. Comminges, C. Morais, Chem. Electro. Chem., **2015**, 2, 1128-1137;

[99] S. Lee, B. Kim, S. Park, Energy, **2014**, 66, 70-76;

[100] C Xu, L Ma, J Li, W Zhao, Z Gan. Int. J. Hydrogen Energy, **2012**, 37, 2985-2992;

[101] S. Ardizzone, C. L. Bianchi, L. Borgese, G. Cappelletti, C. Locatelli, A. Minguzzi, S. Rondinini, A. Vertova, P. C. Ricci, C. Cannas and A. Musinu, J Appl Electrochem , **2009**, 39, 2093-2105;

[102] G. Li, H. Yu, X. Wang, S. Sun, Y. Li, Z. Shao, B. Yi, Phys. Chem.Chem. Phys. **2013**, 15, 2858-2866;

[103] J. Xu, G. Liu, J. Li, X. Wang, Electrochim. Acta, **2012**, 59, 105-112;

[104] Y. Murakami, H. Ohkawauchi, M. Ito, K. Yahikozawa, Y. Takasu, Electrochim. Acta, **1994**, 39, 2551-2554;

[105] C. P. De Pauli, S. Trasatti. Journal of Electroanalytical Chemistry, **2002**, 538-539, 145-151;

[106] A. Marshall, M. Tsypkin, B. Børresen, G. Hagen, and R. Tunold. J. New Mater. Electrochem. Systems, **2004**, 7, 197-204;

[107] A Marshall, B Børresen, G Hagen , S Sunde , M Tsypkin. Russian J. Electrochem., **2006**, 42, 1134-1140;

[108] J. Y. Lim, G. Rahman, S. Y. Chae, K. Lee, C. Kim, O Joo. Int. J. Energy Res, **2014**, 38, 875-883;

[109] X. Wu, J. Tayal, S. Basu and K. Scott, Int. J. Hydrogen Energy, **2011**, 36, 14796-14804;

[110] N. J. Pe´rez-Viramontes, I. L. Escalante-Garcia, C. Guzma´n-Martinez, M. Galvan-Valencia, S. M. Duro´n-Torres, J Appl Electrochem, **2015**, 45, 1165-1173;

[111] S. Ardizzone, C.L. Bianchi, G. Cappelletti, M. Ionita, A. Minguzzi, S. Rondinini, A. Vertova, J. Electroanal. Chem. **2006**, 589, 160-166;

[112] K. Kadakia, M. K. Datta, O. I. Velikokhatnyi, P. Jampani, S. K. Park, P. Saha, J. A. Poston, A. Manivannan, P. N. Kumta. Int. J. Hydrogen Energy, **2012**, 37, 3001-3013;

[113] O. Kasian, S.Geiger, M. Schalenbach, A. M. Mingers, A. Savan, A. Ludwig, S. Cherevko, Karl J. J. Mayrhofer. Electrocatalysis, **2018**, 9, 139-145.

[114] J. Xu, Q. Li, E. Christensen, X. Wang, N. J.Bjerrum, Int. J. Electrochem Sci, **2013**, 8, 2388-2406;

[115] O. I. Velikokhatnyi, K. Kadakia, M. K. Datta and P. N. Kumta. J. Phys. Chem. C **2013**, 117, 20542-20547;

[116] K. Kadakia, M. K. Datta, P. H. Jampani, S. K. Park and P. N. Kumta, J. Power Sources, **2013**, 222, 313-317;

[117] K. S. Kadakia, P. H. Jampani, O. I. Velikokhatnyi, M. K. Datta, S. K. Park, D. H. Hong, S. J. Chung and P. N. Kumta, J. Power Sources, **2014**, 269, 855-865;

[118] M. K. Datta, K. Kadakia, Oleg I. Velikokhatnyi, Prashanth H. Jampani, Sung Jae Chung, James A. Poston, Ayyakkannu Manivannan, Prashant N. Kumta, J. Mater. Chem. A, **2013**, 1, 4026-4037;

[119] K. S. Kadakia, P. Jampani, O. I. Velikokhatnyi, M. K. Datta, S. J. Chung, J. A. Poston, A. Manivannan, P. N. Kumta, J. Electrochem. Soc., **2014**, 161, F868-F875;

[120] K. Kadakia , M. K. Datta , O. I. Velikokhatnyi, P. H. Jampani , P. N. Kumta, Int. J. Hydrogen Energy, **2014**, 39, 664-674;

[121] K. Kadakia, M. K. Datta, O. I. Velikokhatnyi, P. Jampani, S. K. Park , S. J. Chung, P. N. Kumta. Journal of Power Sources, **2014**, 245, 362-370;

[122] S. D. Yim, W. Y. Lee, Y. G. Yoon, Y. J. Sohn, G. G. Park, T. H. Yang, C. S. Kim. Electrochim. Acta, **2004**, 50, 713-718;

[123] F. Ye, J. Li, X. Wang ,T. Wang, S. Li, H. Wei, Q. Li , E. Christensen, Int. J. Hydrogen Energy, **2010**, 35, 8049-8055;

[124] Da Silva, L. A.; Alves, V. A.; Trasatti, S.; Boodts, J. F. C. J. Electroanal. Chem. **1997**,427, 97-104;

[125] D. Seley, K. Ayers and B. A. Parkinson, ACS Comb. Sci. **2013**, 15, 82-89;

[126] M. H. P. Santana, L. D. Faria, J. F. Boodts, J. Applied Electrochemistry, **2005**, 35, 915-924;

[127] A. Bonakdarpour, R. T. Tucker, M. D. Fleischauer, N. A. Beckers, M. J. Brett and D. P. Wilkinson, Electrochim. Acta, **2012**, 85, 492-500;

[128] L. Zhang, L. Y. Wang, C. M. B. Holt, T. Navessin, K. Malek ,M. H. Eikerling and D. Mitlin, J. Phys. Chem. C, **2010**, 114, 16463-16474;

[129] M. Yin, J. Xu, Q. Li, J. O. Jensen, Y. Huang, L. N. Cleemann, N. J. Bjerrum, W. Xing, Appl. Catal. B Environ. , **2014**, 144, 112-120;

[130] X. Wu, K. Scott, Int. J. Hydrogen Energy, **2011**, 36, 5806-5810;

[131] A. T. Marshall, R. G. Haverkamp, Electrochim. Acta, **2010**, 55, 1978-1984;

[132] J.C. Cruz, S. Rivas, D. Beltran, Y. Meas, R. Ornelas, G. Osorio-Monreal, L. Ortiz-Frade, J. Ledesma-Garcia and L.G. Arriaga, Int. J. Hydrogen Energy, **2012**, 37, 13522-13528;

[133] V. K. Puthiyapura, M. Mamlouk, S. Pasupathi, B. G. Pollet, K. Scott, J. Power Sources, **2014**, 269, 451-460;

[134] H. S. Oh, H. N. Nong, P. Strasser, Adv. Funct. Mater. **2015**, 25, 1074-1081;

[135] H. N. Nong, L. Gan, E. Willinger, D. Teschner, P. Strasser. Chem Sci, **2014**, 5, 2955-2963;

[136] H. N. Nong, H.-S. Oh, T. Reier, E. Willinger, M.-G. Willinger, V. Petkov, D. Teschner, P. Strasser, Angew. Chem, **2015**, 127, 3018-3022;

[137] H.-S. Oh, H. N. Nong, T. Reier, A. Bergmann, M. Gliech, J. F. de Araújo, E. Willinger, R. Schlögl, D.Teschner and Peter Strasser, J. Am. Chem. Soc. **2016**, 138, 12552-12563;

[138] J. Tong, Y. Liu, Q. Peng, W. Hu , Q. Wu, J Mater Sci., **2017**, 52, 13427-13443;

[139] F. Karimi, B. A. Peppley, Electrochim. Acta, **2017**, 246, 654-670;

[140] F. Karimi, A. Bazylak and B. A. Peppley, J. Electrochem. Soc, **2017**, 164, F464-F474;

[141] L. Wang, F. Song, G. Ozouf, D. Geiger, T. Morawietz, M. Handl, P. Gazdzicki, C. Beauger, U. Kaiser, R. Hiesgen, A. S. Gago and K. A. Friedrich, J. Mater. Chem. A, **2017**, 5, 3172-3178;

[142] K.-S. Lee, I.-S. Park, Y.-H. Cho, D.-S. Jung, N. Jung, H.-Y. Park, Y.-E. Sung, Journal of Catalysis, **2008**, 258, 143–152.
[143] S. Gurrik. Performance of supported catalysts for water electrolysis, level of M.Sc, Norwegian University of Science and Technology, **2012**;
[144] Aaron T. Marshall • Richard G. Haverkamp. J Mater Sci , **2012**, 47, 1135-1141;
[145] P. Mazur, J. Polonsky, M. Paidar, K. Bouzek, Int. J. Hydrogen Energy, **2012**, 37, 12081-12088;
[146] E. Oakton, D. Lebedev, M. Povia, D. F. Abbott, E. Fabbri, A. Fedorov, M. Nachtegaal, C. Coperet and T. J. Schmidt, ACS Catal., **2017**, 7, 2346-2352;
[147] Z.-X. Lu, Y. Shi, C.-F. Yan, C.-Q. Guo, Z.-D. Wang, Int. J. Hydrogen Energy, **2017**, 42, 3572-3578;
[148] E. Oakton, D. Lebedev, A. Fedorov, F. Krumeich, J. Tillier, O. Sereda, T. J. Schmidt and C. p. Coperet. New J. Chem, **2016**, 40, 1834-1838;
[149] S. L. Gojkovic, B. M. Babic, V. R. Radmilovic and N. V. Krstajic, J.Electroanal. Chem., **2010**, 639, 161-166;
[150] G. Wu, M. A. Nelson, N. H. Mack, S. G. Ma, P. Sekhar, F. H. Garzon and P. Zelenay, Chem. Commun., **2010**, 46, 7489-7491;
[151] S. V. Kraemer, J. Wikander, G. Lindbergh, A. Lundblad and A. E. C. Palmqvist, J. Power Sources, **2008**, 180, 185-190;
[152] J. R. Osman, J. A. Crayston, A. Pratt and D. T. Richens, J. Sol–Gel Sci. Technol., **2008**, 46, 126-132;
[153] J. R. Osman, J. A. Crayston, A. Pratt and D. T. Richens, J. Sol–Gel Sci. Technol., **2007**, 44, 219-225;
[154] C Rozain , E Mayousse , N Guillet , P Millet. Appl. Catal. B: Environ., **2016**, 182, 123-160;
[155] C. H. Comninellis, G. P. Vercesi. J. Appl. Electrochem., **1991**, 21: 335-345;
[156] K. Kameyama, S. Shohji, S. Onoue, K. Nishimura, K. Yahikozawa, and Y. Takasu. J. Electrochem. Sac. , **1993**, 140, 1034-1037;
[157] B. Johnson, F. Girgsdies, G. Weinberg, D. Rosenthal, A. Knop-Gericke, and R. Schlogl, T. Reier and P. Strasser. J. Phys. Chem. C **2013**, 117, 25443-25450;
[158] Z. Chen, S. Zhang, Y. Shao, S Zhou, X. Wu, J. Zhu, D. Tang. Appl. Surface Sci., **2017**, 422, 891-899;
[159] S. Siracusano, V. Baglio, C. D'Urso, V. Antonucci, A.S. Aricò, Electrochim. Acta, **2009**, 54, 6292-6299;
[160] E. Slavcheva, G. Borisov, E. Lefterova, E. Petkucheva and I. Boshnakova, Int. J. Hydrogen Energy, **2015**, 40, 11356-11361;
[161] L. Wang, P. Lettenmeier, U. G.-Schindler, P. Gazdzicki, N. A. Canas, T. Morawietz, R. Hiesgen, S. Schwan Hosseiny, A. S. Gago, K. A. Friedrich. Phys. Chem. Chem.Phys, **2016**, 18, 4487-4495;
[162] C. Hao, H. Lv, C. Mi, Y. Song and J. Ma. ACS Sustainable Chem. Eng, **2016**, 4, 746-756;
[163] W. Hu, S. Chen, Q. Xia, Int. J. Hydrogen Energy, **2014**, 39, 6967-6976;
[164] J. Pettersson, B. Ramsey, D. Harrison. J Power Sources, **2006,** 157, 28-34;
[165] C. Hao, H. Lv, Q. Zhao, Int. J. Hydrogen Energy, **2017**, 42, 9384-9395;
[166] V. K. Puthiyapura, S. Pasupathi, H. Su, X. Liu, B. Pollet and K. Scott, Int. J. Hydrogen Energy, **2014**, 39, 1905-1913;
[167] M. Yagi, E. Tomita, S. Sakita, T. Kuwabara, K. Nagai, J. Phys. Chem. B, **2005**, 109, 21489-21491;
[168] S. Sui, L. Ma and Y. Zhai, J. Chem. Eng., **2009,** 4, 8-11;
[169] L. Ma, S. Sui, Y. Zhai, Int. J. Hydrogen Energy, **2009**, 34, 678-684;
[170] J. Polonsky, P. Mazur, M. Paidar, E. Christensen, K. Bouzek, Int. J. Hydrogen Energy, **2014**, 39, 3072-3078;
[171] Z. Yan, H. Zhang, Z. Feng, M. Tang, X. Yuan and Z. Tan. J. Alloy Compd., **2017**, 708, 1081-1088;
[172] J. Polonsk´y, I.M.M. Petrushina, E. Christensen, K. Bouzek, C.B.B. Prag, J.E.T.E.T. Andersen, Int. J. Hydrogen Energy, **2012**, 37, 2173-2181;
[173] A.V. Nikiforov, A.L. Tomas Garcia, I.M. Petrushina, E. Christensen, N.J. Bjerrum. Int. J. Hydrogen Energy, **2011**, 36, 5797-5805;
[174] N. Baumann, C. Cremers, K. Pinkwart and J. Tübke, Energy Technol, **2016**, 4, 212-220;
[175] D. L. Wang, C. V. Subban, H. S. Wang, E. Rus, F. J. DiSalvo and H. D. Abruna, J. Am. Chem. Soc, **2010**, 132,10218-10220;
[176] H. Chhina, S. Campbell and O. Kesler, J. Electrochem. Soc., **2007**, 154, B533-B539;
[177] F. Kong, S. Zhang, G.-P. Yin, J. Liu. Z. Q. Xu, Int. J. Hydrogen Energy, **2013**, 38, 9217-9222 ;
[178] Y. Zhang, L. Qian, W. Zhao, X. Li, X. Huang, X. Mai, Z. Wang, Q. Shao, X. Yan, Z. Guo. J. Electrochem. Soc. **2018**, 165, H510-H516;
[179] Y. Wang, J. Clancey, G. Lu, J. Liu, L. Liu, J. Chaudhuri, S. George, M. Xie, S. Wei, Z. Guo. J. Electrochem. Soc. **2016**, 163, F1-F10;
[180] Y. Wang, Q. He, H. Wei, J. Guo, K. Ding, Q. Wang, Z. Wang, S. Wei, Z. Guo. Electrochim. Acta, **2015**, 184, 452-465;
[181] K. Ding, Y. Wang, H. Yang, C. Zheng, Y. Cao, H. Wei, Y. Wang, Z. Guo. Electrochim. Acta, **2013**, 100, 147-156;
[182] H. Yu, L. Yang, D. Cheng, D. Cao. Eng. Sci., **2018**, 3, 54-61
[183] L. Wei, K. Lozano, Y. Mao. Eng. Sci., **2018**, 3, 62-66.
[184] L. Wang, V. A. Saveleva, S. Zafeiratos, E. R. Savinova, P. Lettenmeier, P. Gazdzicki, A. S. Gago and K. A. Friedrich, Nano Energy, **2017**, 34, 385-391;
[185] L. C. Seitz, C. F. Dickens, K. Nishio, Y. Hikita, J. Montoya, A. Doyle, C. Kirk, A. Vojvodic, H. Y. Hwang, J. K. Norskov and T. F. Jaramillo, Science, **2016**, 353, 1011-1014;
[186] O. Diaz-Morales, S. Raaijman, R. Kortlever, P. J. Kooyman, T. Wezendonk, J. Gascon, W.T. Fu1 & Marc T.M. Koper. Nat. Commun., **2016**, 7, 12363.
[187] T. Reier, Z. Pawolek, S. Cherevko, M. Bruns, T. Jones, D. Teschner, S. Selve, A. Bergmann, H. N. Nong, R. Schlögl, K. J. J. Mayrhofer, P. Strasser. J. Am. Chem. Soc., **2015**, 137, 13031–13040.
[188] V. Pfeifer, T. E. Jones, J. J. V. V´elez, R.Arrigo, S. Piccinin, M. H¨avecker, A. K.-Gericke and R. Schl¨ogl.. Chem. Sci., **2017**, 8, 2143–2149.
[189] Al. Grimaud, A. Demortière, M. Saubanère, W. Dachraoui, M.Duchamp, M.-L. Doublet and J.-M. Tarascon. Nat. Energy **2016**, 2, 16189.
[190] S. Geiger, O. Kasian, M. Ledendecker, E. Pizzutilo, A. M. Mingers, W. T. Fu, O. D.-Morales, Z. Li, T.s Oellers, L. Fruchter, A. Ludwig, K. J. J. Mayrhofer, Marc T. M. Koper and S. Cherevko. Nature Catalysis, **2018**, 1, 508-515.
[191] G. Beni, L. M. Schiavone, J. L. Shay, W. C. Dautremont-Smith, B. S.Schneider, Nature **1979**, 282, 281–283.
[192] E. J. Frazer, R. Woods, J. Electroanal. Chem. Interfacial Electrochem. **1979**,102, 127–130.
[193] M. Vukovic´, J. Appl. Electrochem. **1987**, 17, 737–745.
[194] Reier, T.; Teschner, D.; Lunkenbein, T.; Bergmann, A.; Selve, S.; Kraehnert, R.; Schlogl, R.; Strasser, P. J. Electrochem. Soc. **2014**, 161, F876-F882.
[195] V. Pfeifer, T. E. Jones, J. J. Velasco V8lez, C. Massu8, R. Arrigo, D. Teschner, F. Girgsdies, M. Scherzer, M. T. Greiner, J. Allan, et al., Surf. Interface Anal.**2016**, 48, 261–273.
[196] V. Pfeifer, T. E. Jones, J. J. Velasco V8lez, C. Massu8, M. T. Greiner, R. Arrigo, D. Teschner, F. Girgsdies, M. Scherzer, J. Allan, et al., Phys. Chem.Chem. Phys. **2016**, 18, 2292–2296.
[197] V. Pfeifer, T. E. Jones, S. Wrabetz, C. Massue, J. J. Velasco Velez, R. Arrigo, M. Scherzer, S. Piccinin, M. Havecker, A. Knop-Gericke, et al., Chem. Sci. **2016**, 7, 6791–6795.
[198] Simon Geiger, Olga Kasian, Buddha R. Shrestha, Andrea M. Mingers, Karl J. J. Mayrhofer, and Serhiy Cherevko. Journal of The Electrochemical Society, **2016**,163, F3132-F3138.
[199] E. Willinger, C. Massué, R. Schlögl, and M. G. Willinger. J. Am. Chem. Soc. **2017**, 139, 12093−12101.
[200] C. Massue, X. Huang, A. Tarasov, C. Ranjan, S. Cap, and R. Schlçgl. ChemSusChem **2017**, 10, 1958-1968.
[201] Z. Pavlovic, C. Ranjan, Q. Gao, M. Gastel, R. Schlögl. ACS Catal. **2016**, 6, 8098−8105;
[202] E. Antolini, ACS Catal, **2014**, 4, 1426-1440.

10.1002/cssc.201802873

WILEY-VCH

REVIEW

This is the SPE water electrolysis principle diagram of the structure. Water electrolysis at anode produces O_2 and four protons near the electrode surface for each oxygen molecule. Hydrogen ions through the PEM generate H_2 gas near the cathode. The electrocatalyst are directly attached to the membrane to form the SPE composite membrane electrode.

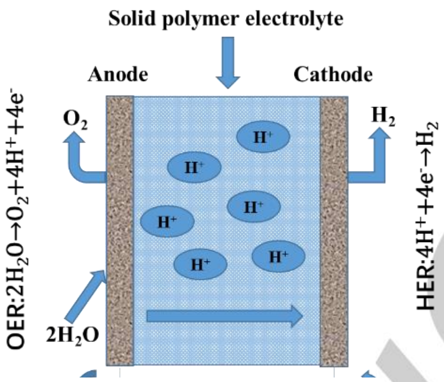

Chao Wang, * *Feifei Lan, Zhenfeng He,* * *Xiaofeng Xie,* * *Yuhong Zhao, Hua Hou, Li Guo, Vignesh Murugadoss, Hu Liu, Qian Shao, Qiang Gao,***Tao Ding,* * *Renbo Wei,* Zhanhu Guo**

Page No. – Page No.

Title: Iridium-based Catalysts for Solid Polymer Electrolyte Electrocatalytic Water Splitting.

Table 1 A review of OER activity on the materials, methods, and components used in SPE water electrolysis in many publications over the years

Refs	Anode catalyst	Cathode catalyst	Anode loading mg cm^{-2}	Cathode loading mg cm^{-2}	Mem	Cell area /cm^2	Pressure /atm	T/^{o}C	E/V@1 A cm^{-2}	method of anode catalyst preparation	water flow rate
[33]	IrO_2	Pt	2.5	0.4	-	7	1	90	1.7	-	
[35]	IrO_2	Pt	0.5	0.25	N.115	25	1	80	1.72		200/mL h^{-1}
[38]	IrO_2	Pt/C-Baltic	2	2	Aquivion@ $_{(120μm)}$	6.25	3 bar	120	1.57	hydrolysis	
[40]	IrO_2	10%Pt/C_{XC72}	2	0.4	-	5		80	1.65		
[42]	IrO_2	Pt/C	3	0.5	N.112	5	1	80	1.63	colloid	
[42]	IrO_2	Pt/C	3	0.5	N.112	5	1	80	1.66	Adams	
[44]	IrO_2	40%Pt/C	1.5	0.5	N.212	5	1	80	1.62	Adams	
[46]	IrO_2	30%Pt/C_{XC72}	3	0.6	N.115	5	1	80	1.7	Colloid	
[54]	IrO_2/CP	Pt/C	0.1	0.4	N.212	4	1	90	1.6	electrodeposition	
[57]	IrO_2(SBA-15)	40%Pt/C_{JM}	1.5	1	N.115	5	1	90	1.629	hard template	
[59]	Ir-ND/ATO	46Pt/C_{TKK}	Total noble metal loading :1		N.212	5	1	80	1.67	Reduction method	1.5mL min^{-1}
[66]	$Ru_{0.9}Ir_{0.1}O_2$	46.1%Pt/C_{TKK}	2.5	0.4	N.115	25	10 bars	60	1.88	thermal decomposition	
[67] √	$Ru_{0.8}Ir_{0.2}O_2$	46.1%Pt/C_{TKK}	2.5	0.4	N.115	5	1	25	1.8	thermal decomposition	
[70]	$Ir_{0.2}Ru_{0.8}O_2$	28.4%Pt/C	Total noble metal loading :1.7		N.1035	5	1	80	1.622	Adams	
[72] √	$Ir_{0.7}Ru_{0.3}$Ox	30%Pt/C	1.5	0.5	N.115	5	1	90	1.57	Adams	4mL min^{-1}
[77]	$Ir_{0.7}Ru_{0.3}O_x$	30%Pt/C_{XC72}	1.5	0.5	Aquivion® $_{(120μm)}$	5	1	90	1.56	Adams	2mL min^{-1}
[78]	$Ir_{0.5}Ru_{0.5}O_x$	--	3	--	N.115	5	1	80	--	--	40mL min^{-1}
[79]	$Ir_{0.7}Ru_{0.3}O_x$	30%Pt/C_{XC72}	Total noble metal loading :1.6		Aquivion®$_{(90μm)}$	5	1	80	1.58	Adams	4mL min^{-1}
[83]	$Ru_{0.8}Ir_{0.2}O_2$	46.1%Pt/C_{TKK}	1~1.6	0.2	N.117	25	1	80	1.739	co-precipitation	--
[91] √	$Ir_{0.6}Ru_{0.4}O_2$	20%Pt/C_{XC72}	2	0.4	N.115	5	--	80	1.567	aqueous hydrolysis	5mL min^{-1}
[93]	IrO_2	20%Pt/C_{XC72}	2	0.4	N.115	5	--	90	1.61	modified polyol	--
[93]	$Ir_{0.8}Sn_{0.2}O_2$	20%Pt/C_{XC72}	2	0.4	N.115	5	--	80	1.642	polyol	--
[96]	$Ir_{0.4}Ru_{0.6}O_2$	28.4%Pt/C_{TKK}	1.5	0.5	N.1035	5	--	80	1.646	Adams	--
[96]	$Ir_{0.4}Ru_{0.6}Mo_xO_y$	28.4%Pt/C_{TKK}	1.5	0.5	N.1035	5	--	80	1.606	Adams	--
[100]	$Ru_{0.3}Ir_{0.7}O_2/Pt_{0.15}$	40%Pt/C_{JM}	1.8	0.3	N.117	20	--	60	1.76	two-step method	
[102]	$Ir_{0.52}Sn_{0.48}O_2$	70%Pt/C	1.5	0.57	N.115	5	--	80	1.631	surfactant-assistant method	
[103]	IrO_2/SnO_2 (2:1)	40%Pt/C_{JM}	1.5	0.5	N.212	1	--	80	1.64	Adams	
[114]	Pt-IrO_2/SnO_2	40%Pt/C_{JM}	1.2	0.5	N.212	1.5	1	80	1.533	chemical reduction	
[117]	IrO_2:10 wt.% F	Pt black $_{SA}$	--	--	N.115	5*5	1	50	1.95	Adams	
[130]	RuO_2/ATO	50%Pt/C_{AA}	10	1	N.212	--	-	80	1.56	colloid	1~3cm^3 mL^{-1}

Refs	Anode catalyst	Cathode catalyst	Anode loading mg cm^{-2}	Cathode loading mg cm^{-2}	Mem	Cell area /cm^2	Pressure /atm	T/^{o}C	E/V@1 A cm^{-2}	method of anode catalyst preparation	water flow rate
[133]	90% IrO_2-ATO	20%Pt/C_{AA}	2	0.5	N.115	1	1	80	1.73	Adams	
[133]	80% IrO_2-ATO	20%Pt/C_{AA}	2	0.5	N.115	1	1	80	1.74	Adams	
[133]	60% IrO_2-ATO	20%Pt/C_{AA}	2	0.5	N.115	1	1	80	1.8	Adams	
[133]	40% IrO_2-ATO	20%Pt/C_{AA}	2	0.5	N.115	1	1	80	1.96	Adams	
[145]	60%IrO_2/$TiO_{2.(R200M)}$	Pt	0.9	0.5	N.117	4	3 bars	120	1.67	Adams	
[154]	50% IrO_2/Ti	46%Pt/C_{TKK}	0.2	0.25	N.115	25	1	80	1.73	--	--
[160]	Ir/Ebonex	20%Pt/C_{XC72}	0.2	0.2	N.117	25	1	80	1.74	Sol-gel	--
[162]	40I/TN-20	40%Pt/C_{JM}	2.5	0.5	N.117	3.645	1	80	2.027	EISA	40mL min^{-1}
[165]	40Ir/TV-20	40%Pt/C_{JM}	2.5	0.5	N.117	3.645	1	80	2.015	EISA	40mL min^{-1}
[166]	90% IrO_2-ITO	20%Pt/C_{AA}	2	0.5	N.115	1	1	80	1.74	Adams	
[166]	60% IrO_2-ITO	20%Pt/C_{AA}	2	0.5	N.115	1	1	80	1.78	Adams	
[166]	IrO_2	20%Pt/C_{AA}	2	0.5	N.115	1	1	80	1.73	Adams	
[168]	Ir/TiC (40 wt% Ir)	40%Pt/C_{JM}	1.5	1	N.112	20	1	80	1.8		10mL min^{-1}
[169]	20% Ir/TiC	Pt	1.5	1	N.112	20	1	80	1.85		10mL min^{-1}
[184]	$Ir_{0.7}Ru_{0.3}O_x$(EC)	40% Pt/C	1	0.4	N.212	50	1	80	1.68		
[184]	$Ir_{0.7}Ru_{0.3}O_x$(TT)	40% Pt/C	1	0.4	N.212	50	1	80	1.74		

Abbreviations: JM= Johnson Matthey; N. =Nafion®; AA= Alfa Aesar; SA=Sigma Aldrich; TKK=Tanaka; C= carbon Vulcan XC-72; √ = iR correction; EISA= evaporation-induced self-assembly method